Precambrian Research xxx (2011) xxx–xxx

Contents lists available at ScienceDirect

Precambrian Research

journal homepage: www.elsevier.com/locate/precamres

UHT sapphirine granulite metamorphism at 1.93–1.92 Ga caused by gabbronorite intrusions: Implications for tectonic evolution of the northern margin of the North China Craton

JingHui Guo[a,*], Peng Peng[a], Yi Chen[a], ShuJuan Jiao[a], Brian F. Windley[b]

[a] State Key Laboratory of Lithospheric Evolution, Institute of Geology and Geophysics, Chinese Academy of Sciences, Beijing, 100029, China
[b] Department of Geology, The University of Leicester, Leicester, LE1 7RH, UK

ARTICLE INFO

Article history:
Received 31 March 2011
Received in revised form 25 July 2011
Accepted 28 July 2011
Available online xxx

Keywords:
Sapphirine granulite
Ultrahigh-temperature (UHT) metamorphism
P–T path
Palaeoproterozoic
Khondalite belt
North China Craton

ABSTRACT

Sapphirine granulites occur in the Daqingshan and Jining areas in the Palaeoproterozoic Khondalite belt, which divides the Western Block of the North China Craton into the Yinshan block to the north and the Ordos block to the south. The sapphirine granulites in the Daqingshan area are always in contact with meta-gabbronorite dykes, implying a causal relationship. The sapphirine-bearing rocks are divided into spinel–garnet–sillimanite–biotite–plagioclase–sapphirine gneiss, UHT sapphirine granulite, and spinel–garnet granulite. The sapphirine granulite contains up to 30% sapphirine, garnet (30–50%), spinel (5–15%), sillimanite (5–15%), biotite (10–20%) and plagioclase (10–20%) with minor cordierite, rutile and ilmenite, but without quartz and orthopyroxene. Bulk chemical compositions show that the sapphirine granulites have very low SiO_2 contents (39 wt.%), high Al contents, and low X_{Mg}. Biotite contains very high TiO_2 contents up to 7.6 wt.%. Detailed petrographic examination of the sapphirine granulites reveals five mineral assemblages (M_0–M_4): (1) an assemblage (M_0) of mineral inclusions within garnet cores, (2) a matrix (peak) assemblage (M_1) represented by coarse-grained garnet, sapphirine, spinel, sillimanite, biotite and plagioclase, (3) sapphirine + plagioclase symplectite (M_2), (4) spinel + plagioclase symplectite (M_3), and (5) retrogressive biotite (M_4). The *P–T* stability field in the pseudosection of the NCKFMASH system indicates that the temperature of the peak UHT metamorphism of the Daqingshan sapphirine granulites is in the range 910–980 °C (this compares with the peak regional metamorphic temperature of the khondalites of 700–820 °C). The *P–T* path inferred from the *P–T* stability fields of the mineral assemblages (M_1–M_4) suggests that the peak UHT metamorphism (M_1) was followed by nearly isothermal decompression (M_2 and M_3) and later cooling (M_4). Field relations and geochronological data suggest that the high-heat flow necessary for the UHT metamorphism of the sapphirine granulites from the Daqingshan area was provided by coeval ~1.93–1.92 Ga gabbronorite intrusions that were most probably generated by ridge subduction, which was also responsible for abundant garnet-rich granites by crust melting the area.

© 2011 Elsevier B.V. All rights reserved.

1. Introduction

Silica-undersaturated sapphirine-bearing granulites, an important and distinctive type of ultrahigh-temperature (UHT) metamorphic rocks, have been reported from a number of high-grade terrains worldwide including: Antarctica, India, Sri Lanka, Australia, South Africa, Algeria, Canada, Brazil, Italy, Norway, Scotland, Japan, and Peru (see Kelsey et al., 2005; Kelsey, 2008 and references therein). Such rocks are mineralogically and texturally complex, and document abundant metamorphic reactions and derivative processes that provide important insights into understanding the tectonothermal evolution of UHT metamorphism (Harley, 1989, 1992, 1998a,b,c; Kelsey et al., 2005; Kelsey, 2008). Although UHT is now generally accepted as a part of regional crustal orogenesis, there is still in controversy on the relations of UHT rocks with other rocks, their tectonic settings, and the geodynamic models that have been proposed, i.e., back-arc basins, ridge subduction, self heating of the orogen, accretionary or collisional orogens (e.g. Brown, 2006, 2007a,b, 2009; Kelsey, 2008; Santosh and Kusky, 2010). Therefore it is timely and necessary to document in detail further examples, as in the North China Craton, where new relations suggest a specific metamorphic history and tectonic setting.

In the North China Craton sapphirine granulites have been described from two localities: the Daqingshan area (Jin, 1989; Liu et al., 1993, 2000; Guo et al., 2006; Wan et al., 2009), and the Jining area (Santosh et al., 2006, 2007a,b; Liu et al., 2010). Both locations

* Corresponding author. Tel.: +86 (0)10 82998541; fax: +86 (0)10 62010846.
E-mail address: jhguo@mail.iggcas.ac.cn (J. Guo).

0301-9268/$ – see front matter © 2011 Elsevier B.V. All rights reserved.
doi:10.1016/j.precamres.2011.07.020

Please cite this article in press as: Guo, J., et al., UHT sapphirine granulite metamorphism at 1.93–1.92 Ga caused by gabbronorite intrusions: Implications for tectonic evolution of the northern margin of the North China Craton. Precambrian Res. (2011), doi:10.1016/j.precamres.2011.07.020

are situated in the EW-trending, Palaeoproterozoic, ~1.95 Ga Khondalite belt, which separates the Yinshan block to the north from the Ordos block to the south (Zhao et al., 2003a, 2005, 2010; Yin et al., 2009, 2011; Zhou et al., 2010). In the Jining area Santosh et al. (2006, 2007a,b, 2008, 2009a,b, 2010) demonstrated that the UHT metamorphism occurred at about ~1.92 Ga, with an anticlockwise *P–T* path. Although the timing of the UHT metamorphism is broadly coincident with that of the collisional event that led to formation of the Khondalite belt, the UHT anticlockwise *P–T* evolution is inconsistent with published clockwise *P–T* paths documented by non-UHT rocks in the Khondalite belt (Jin et al., 1991; Liu et al., 1993, 1997; Lu et al., 1992; Zhao et al., 1999; Wang et al., 2011). Thus, the significance of the UHT metamorphism of the sapphirine granulites in the Khondalite belt remains ambiguous. Compared with the Jining area, the sapphirine granulites in the Daqingshan area are more silica-undersaturated and preserve mineral assemblages and reaction textures that formed during the peak and exhumation stages.

In this study, we present detailed textural and compositional data on mineral assemblages, symplectites and coronas from silica-undersaturated sapphirine granulites from the Daqingshan area. Using the THERMOCALC program (Holland and Powell, 1998), we estimate the *P–T* conditions of the UHT metamorphism and define the ambient *P–T* trajectory. In combination with the field relationships of the sapphirine granulites and their adjacent rocks, our results place new constraints on the origin of the UHT metamorphism and on the tectonic evolution of the Khondalite belt in the Western Block of the North China Craton.

2. Geological setting

It is widely accepted that the North China Craton formed by collisional amalgamation of the Eastern and the Western Blocks along the central Trans-North China Orogen (TNCO) at ~1.85 Ga (Fig. 1; Zhao et al., 1998, 1999, 2000, 2001a, 2002a; Zhao, 2001; Wilde et al., 2002; Guo et al., 2005; Kröner et al., 2005, 2006; Zhang et al., 2007, 2009; Lu et al., 2008; Wang et al., 2010a; Li et al., 2010; Liu et al., 2011), though some other models have also been proposed for the formation and evolution of the craton (Kusky and Li, 2003; Kusky et al., 2007; Li and Kusky, 2007; Faure et al., 2007; Trap et al., 2007; Wang, 2009, 2010; Wang et al., 2010b). The TNCO is 100–300 km wide and ~1500 km long, and in the north it contains widespread high-pressure granulites and retrograde eclogites with clockwise *P–T* paths involving near-isothermal decompression (Zhai et al., 1993, 1996). The presence of these HP rocks is considered as robust evidence for continental collision between the Eastern and Western Blocks to form the TNCO (Zhao et al., 2001b; Guo et al., 2002; Zhang et al., 2006; Xia et al., 2009; Zhao, 2009).

The Palaeoproterozoic Khondalite belt (Fig. 1) occurs within the Western Block of the North China Craton between the Yinshan block to the north and the Ordos block to the south (Zhao et al., 1999, 2005). This EW-trending 1000 km-long Belt extends from the Jining complex in the east via the Daqingshan–Ulashan complex to the Qianlishan and Helanshan complexes in the west (Figs. 1 and 2). The Khondalite belt consists predominantly of quartzo-feldspathic gneiss, garnet quartzite, graphite-bearing sillimanite garnet gneiss (khondalite), marble and calc-silicate rocks together with minor amphibolite and mafic granulite.

The term 'khondalite' refers to an aluminous, meta-pelitic, sillimanite–garnet–quartz paragneiss that also contains graphite, spinel, biotite, feldspar, and/or cordierite, and is common in the North China Craton (Lu et al., 1992, 1996; Condie et al., 1992). In some Chinese literature these rocks were referred to collectively as the meta-sedimentary 'khondalite series' (Jin et al., 1991; Lu et al., 1992, 1996; Qian and Li, 1999), the protoliths of which were considered to have formed and been metamorphosed both in the Neoarchean. However, recent LA-ICP-MS U–Pb zircon dating has demonstrated that detrital zircons from the khondalites were mainly derived from a 2.1–1.96 Ga provenance (Xia et al., 2006a,b, 2008). Protoliths of the Khondalite belt are widely considered to have formed on a passive continental margin (Condie et al., 1992; Li et al., 2000; Xia et al., 2006a,b, 2008), although Wan et al. (2009) favoured an active continental margin or back-arc setting.

Metamorphic zircons from the khondalites have a U–Pb age of ~1.95 Ga, which is interpreted to reflect the age of regional metamorphism (Wan et al., 2006; Santosh et al., 2007b; Yin et al., 2009). This age is consistent firstly with the presence of carbonatite dykes (from 10 cm to several metres wide and up to several hundred metres long) with zircons that have a SHRIMP U–Pb age 1951 ± 5 Ma, which were considered by Wan et al. (2008) to be the product of anatexis of impure marbles in the khondalites, and secondly with the metamorphic age of 1.95 Ma of the Qianlishan complex (Yin et al., 2009). The age of UHT metamorphism in the Jining area was documented by Santosh et al. (2007a) as 1917 ± 48 Ma from monazite dates, and by Santosh et al. (2007b) as 1919–1923 Ma from zircon dates. The Khondalite belt also contains TTG gneisses, meta-gabbros, meta-diorites, syntectonic charnockites and S-type garnet-bearing granitoids; in some areas (e.g. Jining) S-type garnet-rich granites make-up 40% of the total exposure.

3. The Daqingshan Sapphirine granulites

The silica-undersaturated sapphirine-bearing granulites in the Daqingshan area are located in the easternmost part of the Daqingshan–Ulashan complex, which is separated from the Archaean Wuchuan complex to the north by the Jiuguan-Xiashihao Fault (Figs. 2 and 3). Being part of the Archaean Yinshan block, the Wuchuan complex consists of late Archaean TTG gneisses and minor mafic granulites; the latter contain garnet + quartz symplectitic coronas surrounding plagioclase and pyroxene grains (the so-called 'red socket texture' in Chinese literature; Jin et al., 1991). These 'red-socket' textured granulites have a metamorphic age of ~2.5 Ga, and they are characterized by anticlockwise *P–T* paths demonstrating isobaric cooling (Jin et al., 1991). As part of the Palaeoproterozoic Khondalite belt, the Daqingshan–Ulashan complex consists predominantly of meta-sedimentary khondalites together with minor amphibolites and mafic granulites. The metamorphism is characterized by clockwise *P–T* paths that indicate near-isothermal decompression (Liu et al., 1993).

Silica-undersaturated sapphirine granulites crop out around Dongpo village in the Daqingshan area, Wuchuan County, Inner Mongolia (Fig. 3). Predominant rocks in the area are granulite facies, quartzo-feldspathic gneisses that contain conformable layers up to about 800 m thick and 20 km long of meta-pelites and associated marbles and calc-silicate rocks (Fig. 3). At Dongpo the sapphirine granulites occur in a linear belt that is about 10 m wide against a gabbronorite (Fig. 4). At 1.5 km southeast of Dongpo village (Fig. 3), typical sapphirine granulites form a 8–15 m-wide layer (Fig. 4) that contains three lithologies: (1) spinel–garnet–sillimanite–biotite–plagioclase–sapphirine gneiss (2) predominant UHT sapphirine granulite (3) spinel–garnet granulite that forms a discontinuous ~10 cm-wide layer between a gabbronorite and the sapphirine granulite.

The most important in this description is the widespread occurrence in the sapphirine granulites of dykes/sills (some with discordant apophyses) and small discordant and/or conformable round plutons of meta-gabbronorite – hereafter referred to as gabbronorite (Guo et al., 2001; Peng et al., 2005, 2010). There are hundreds of gabbronorite intrusions in the Khondalite belt, especially in the Jining area (not recorded by Santosh et al., 2007a,b;

Please cite this article in press as: Guo, J., et al., UHT sapphirine granulite metamorphism at 1.93–1.92 Ga caused by gabbronorite intrusions: Implications for tectonic evolution of the northern margin of the North China Craton. Precambrian Res. (2011), doi:10.1016/j.precamres.2011.07.020

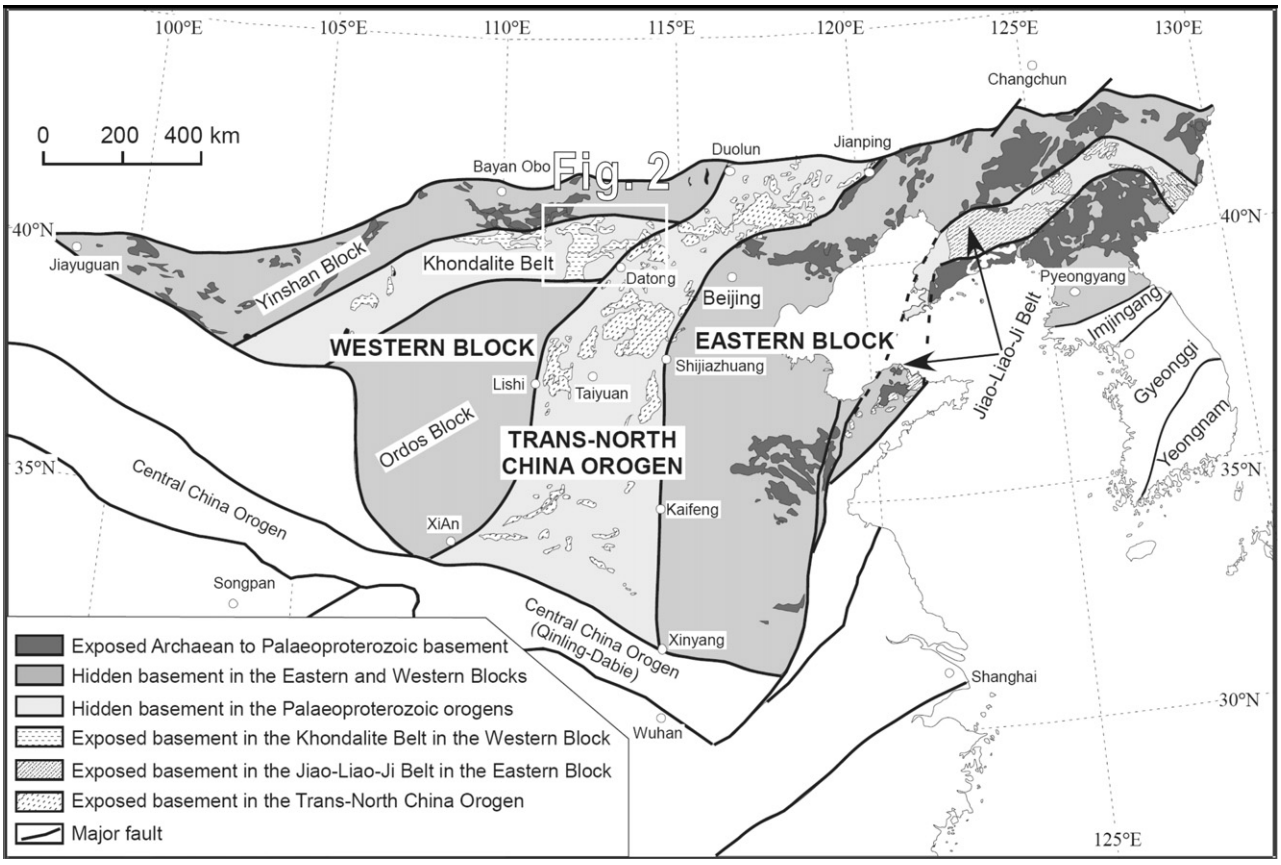

Fig. 1. Tectonic framework of the North China Craton showing the location of the Khondalite belt in the Western Block (after Zhao et al., 2005).

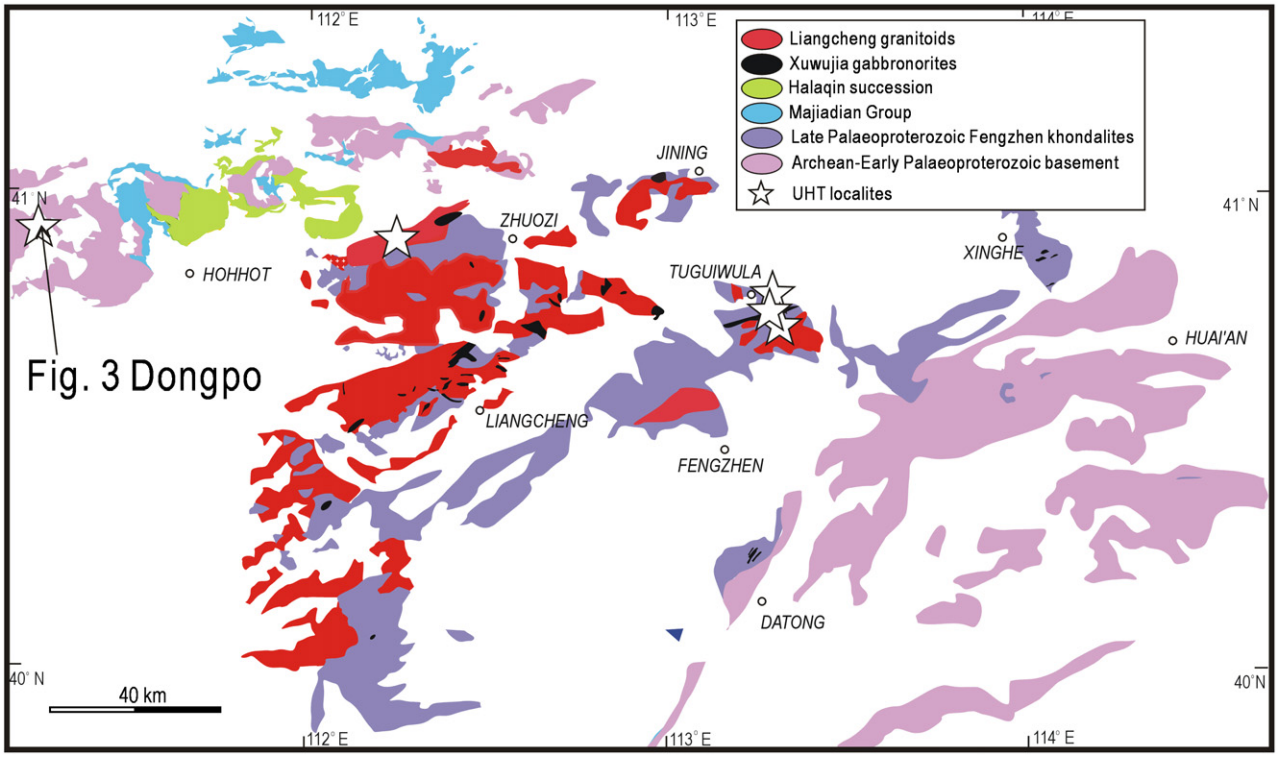

Fig. 2. Simplified geological map of the study area (revised after Peng et al., 2010). The outcrops with ultrahigh-temperature (UHT) granulite are shown with stars. Locality of Fig. 3 marked.

Please cite this article in press as: Guo, J., et al., UHT sapphirine granulite metamorphism at 1.93–1.92 Ga caused by gabbronorite intrusions: Implications for tectonic evolution of the northern margin of the North China Craton. Precambrian Res. (2011), doi:10.1016/j.precamres.2011.07.020

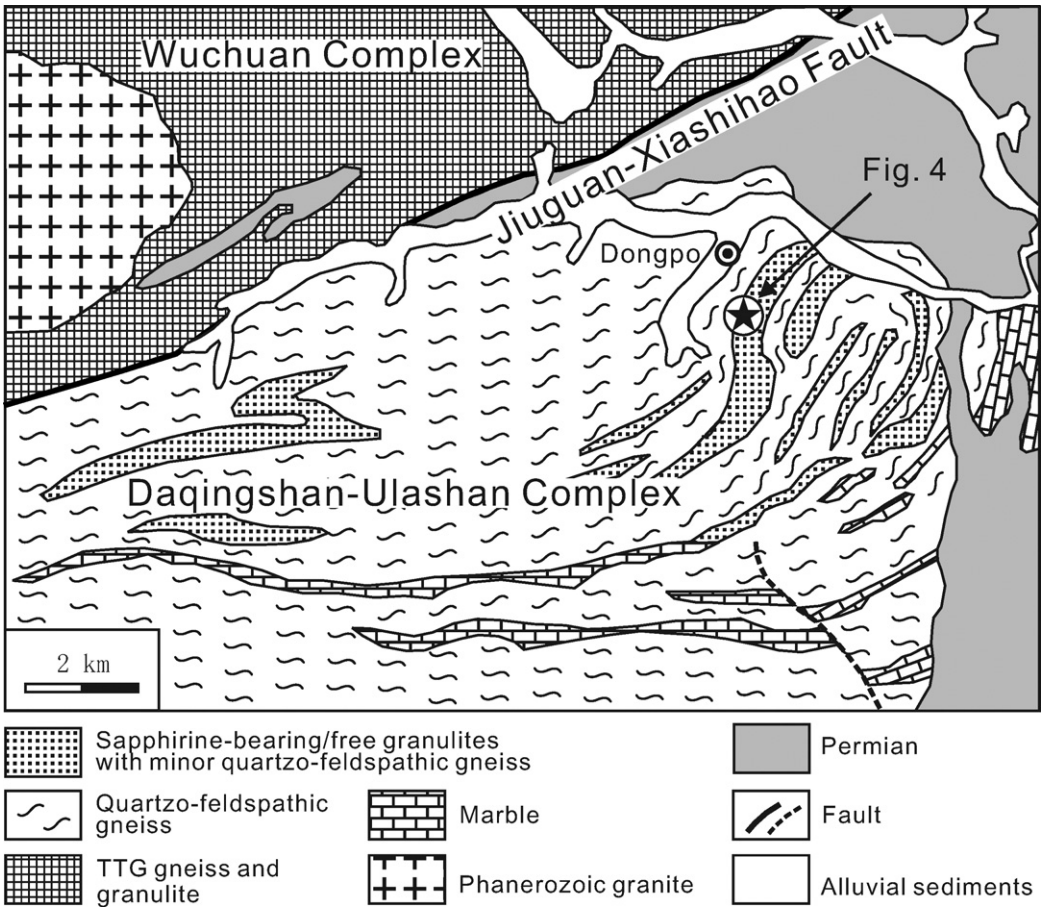

Fig. 3. Geological map of the Dongpo Village area, Daqingshan, Inner Mongolia. The Archaean Wuchuan Complex of the Yinshan Block is separated from the Palaeoproterozoic Daqingshan–Ulashan Complex of the Khondalite belt by the Jiuguan-Xiashihao Fault. Meta-pelitic granulites and marbles occur as layers in quartzo-feldspathic gneisses. Position of Fig. 4 indicated (Simplified after the regional geological map of Dongpo).

Liu et al., 2010). They generally have widths of several meters to hundreds of metres and the largest ones in the Jining area are 1–2 km wide and 5–10 km long. At Dongpo a prominent dyke is c. 20 m wide, and the adjacent sapphirine granulite is parallel to and extends for c. 10 m from the contact of the dyke. The small intrusions mostly consist of gabbronorite, but the large ones range in composition from norite, olivine gabbronorite, quartz gabbronorite, monzonorite, and quartz monzonorite. They are typically composed of hypersthene, clinopyroxene, hornblende, plagioclase ± K-feldspar, and olivine or quartz. Cores and rim of zircons in one gabbronorite dyke have $^{207}Pb/^{206}Pb$ mean ages of 1954 ± 6 Ma and 1925 ± 8 Ma respectively, which constrain the age of mafic magmatism at ~1.95–1.92 Ga (Peng et al., 2010).

Of particular importance is the fact that all UHT rocks are bordered by gabbronorite intrusions, as at the key locations Dongpo, Tuguiwula and Xuwujia (Fig. 2), and many, but not all, gabbronorite intrusions are bordered by UHT sapphirine granulites. Commonly, but not always, there is a similarity between the size of the gabbronorites and the size of the adjacent sapphirine granulites, but dykes of more intermediate monzonitic composition are not usually bordered by sapphirine granulites. Fig. 4a–b shows a 12–20 m-wide gabbronorite sill bordered by a 8–15 m-wide sapphirine granulite layer within a host quartzo-feldspathic gneiss. This sill that continues along strike for at least 300 m was injected between a pelitic layer (the protolith of the sapphirine granulite) and the quartzo-feldspathic gneiss. The gabbronorite shows an ophitic texture with mineral assemblage of plagioclase, clinopyroxene, orthopyroxene and hornblende, without foliation. On its western side the sapphirine-bearing granulite layer is separated from quartzo-feldspathic gneiss by a 1 m-thick quartz + plagioclase vein/dyke (Fig. 4a–b). Smaller rootless quartz + plagioclase veins also occur within the sapphirine-bearing granulite layer. All the quartz + plagioclase veins show a weak foliation defined by elongate quartz and plagioclase; our interpretation is that the veins were generated by partial melting of the pelitic protolith.

The gabbronorites also occur as innumerable round lenses in garnet-rich granitoids; also there are many lenses, commonly about 10–30 cm long, of hybrid granitoids in many gabbronorites (Peng et al., 2010). The granitoids are peraluminous, and composed of plagioclase, K-feldspar, garnet, quartz, and minor hypersthene and clinopyroxene, and have been interpreted as S-type granites derived by partial melting of the khondalites (e.g. Guo et al., 1999; Zhong et al., 2006). Peraluminous granitoids from the 250 km × 100 km Liangcheng pluton/batholith (Fig. 2) have U–Pb zircon SHRIMP ages in the range of 1.93–1.89 Ga (Guo et al., 2001; Zhong et al., 2007). Peng et al. (2010, 2011) concluded that the gabbronorites and the granitoids were products of the same thermal event.

The gabbronorite intrusions have been metamorphosed and deformed. The thinnest dykes are highly deformed and completely recrystallized, whereas the largest plutons have foliated and metamorphosed margins, and relict gabbroic textures and lath-shaped plagioclases in their centers.

The rims of some metamorphic zircons in the sapphirine granulites have SHRIMP zircon ages of c. 1.86 Ma, and metamorphic zircons in the km-size Xigou layered hornblende (after clinopyroxene)–plagioclase gabbro (this is not a gabbronorite intrusion) have a $^{207}Pb/^{206}Pb$ mean age of 1857 ± 4 Ma (Peng et al., 2010).

Please cite this article in press as: Guo, J., et al., UHT sapphirine granulite metamorphism at 1.93–1.92 Ga caused by gabbronorite intrusions: Implications for tectonic evolution of the northern margin of the North China Craton. Precambrian Res. (2011), doi:10.1016/j.precamres.2011.07.020

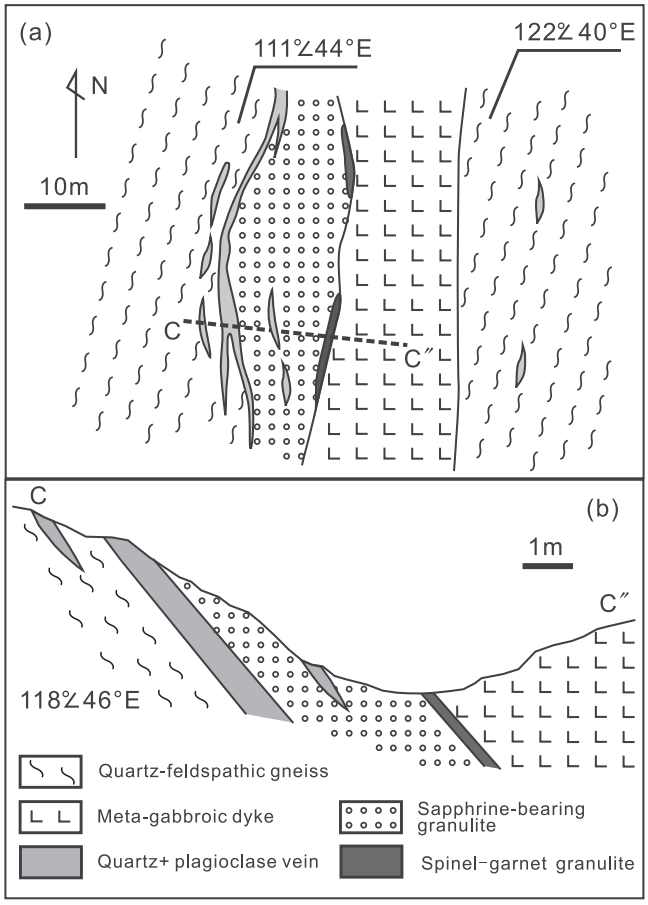

Fig. 4. (a) A geological field map showing a layer of sapphirine granulite and associated rocks on the margin of a meta-gabbronorite sill, all within quartzo-feldspathic gneiss. 1.5 km southeast of Dongpo village (b). A section, C–C", across the rocks shown in Fig. 4a.

4. Petrography and metamorphic textures

Of three types of rocks in the sapphirine granulite layer, only the spinel–garnet–sillimanite–biotite–plagioclase–sapphirine gneisses and the spinel–garnet granulites contain tiny sapphirine grains sparsely disseminated within garnet porphyroblasts, whereas the sapphirine granulite contains numerous grains of sapphirine up to 30% in some samples. Other major phases in the sapphirine granulites are garnet (30–50%), spinel (5–15%), sillimanite (5–15%), biotite (10–20%) and plagioclase (10–20%), with minor cordierite, rutile and ilmenite/magnetite; quartz and orthopyroxene are absent.

Detailed petrographic studies reveal that the sapphirine granulites contain five mineral assemblages (M_0–M_4): (1) an inclusion assemblage (M_0) of well-preserved mineral inclusions within garnet cores, (2) a matrix assemblage (M_1) represented by coarse-grained garnet, sapphirine, spinel, sillimanite, biotite and plagioclase, (3) sapphirine + plagioclase symplectite (M_2), (4) spinel + plagioclase symplectite (M_3), and (5) retrogressive biotite (M_4).

4.1. Inclusion assemblage (M_0)

In the sapphirine granulites some large (5–30 mm) garnet porphyroblasts consist of an inclusion-rich core surrounded by an inclusion-free rim (Fig. 5a–b). The contrasting core–rim texture implies that the garnet cores and rims developed in different metamorphic stages. We consider that the garnet core developed coevally with its enclosed minerals, assigned to the mineral inclusion assemblage (M_0), whereas the garnet rim formed coevally with the matrix minerals. The minerals enclosed in the garnet cores are sillimanite, spinel, biotite, plagioclase, rutile and ilmenite (Fig. 5a–c). The inclusion assemblage (M_0) can also be found in the spinel–garnet granulites (Fig. 5d). Unlike the Jining sapphirine granulites that contain garnets with spinel + quartz inclusions (Santosh et al., 2006), the sapphirine granulites from the Daqingshan area do not contain any quartz inclusions in garnet, and thus we do not know if the M_0 assemblage developed during the prograde stage of the ultrahigh-temperature metamorphism or formed in an earlier metamorphic event unrelated to the ultrahigh-temperature metamorphism.

4.2. Matrix assemblage (M_1)

Abundant coarse-grained sapphirine is the characteristic matrix mineral of the sapphirine granulites; other matrix minerals are garnet, spinel, sillimanite, biotite and plagioclase (Fig. 6a–c), with minor rutile and ilmenite but without orthopyroxene and quartz. In some samples, around the inclusion-free garnet rims are small, euhedral garnet grains that also do not contain any inclusions (Fig. 5b), suggesting that they may have formed coevally with the formation of the garnet rim. Thus, the typical matrix mineral assemblage is sapphirine + spinel + sillimanite + biotite + plagioclase + garnet (the rims and the small euhedral single grains).

Most sapphirines are big, anhedral and enclose many other minerals, which imply that the sapphirine growth reactions controlled the development of the matrix textures. In places garnet and spinel are completely surrounded by sapphirine (Fig. 6a–b), indicating their contributions to the development of the matrix-type sapphirine. Coarse-grained sillimanite is ubiquitous. Biotite occurs with all other matrix minerals, and because no K-feldspar is present in the matrix, biotite is the sole potassium-bearing phase in the matrix assemblage (M_1). Although minor plagioclase grains occur randomly, most plagioclase is in contact with or nearby garnet and sapphirine. In addition, some plagioclase occurs as a corona surrounding garnet (Fig. 6a–b). These textural relations suggest that plagioclase was a major Ca- and Na-bearing mineral phase in the matrix mineral-forming stage, and that small amounts of plagioclase were produced by the breakdown of garnet.

Because granular garnet, spinel and sillimanite never occur together, and sapphirine often contains garnet and spinel inclusions, we infer that the matrix-type sapphirine was produced by the consumption of garnet, spinel and probably sillimanite, and the elimination of one of the three reactant minerals in certain domains stopped the sapphirine-producing reaction. Fig. 6a–c shows the textural evidence for the development of sapphirine from the consumption of garnet, spinel and sillimanite.

4.3. Sapphirine + plagioclase symplectite (M_2)

Sapphirine + plagioclase symplectites occur around garnet, sillimanite and biotite (Fig. 6c–f). Five textural types of sapphirine + plagioclase symplectite have been recognized based on their bordering host minerals. They are present (1) around garnet (Fig. 6c), (2) around matrix-type sillimanite, (3) between garnet and sillimanite (Fig. 6d), with more plagioclase on the garnet side and more sapphirine on the sillimanite side, (4) around biotite (Fig. 6e), and (5) as an isolated narrow band (Fig. 6f). The most common sapphirine + plagioclase symplectites are around garnet or between garnet and sillimanite. The presence of the sapphirine + plagioclase symplectites around biotite (Fig. 6e) indicates that some of the matrix-type biotite broke down during the M_2 stage.

Please cite this article in press as: Guo, J., et al., UHT sapphirine granulite metamorphism at 1.93–1.92 Ga caused by gabbronorite intrusions: Implications for tectonic evolution of the northern margin of the North China Craton. Precambrian Res. (2011), doi:10.1016/j.precamres.2011.07.020

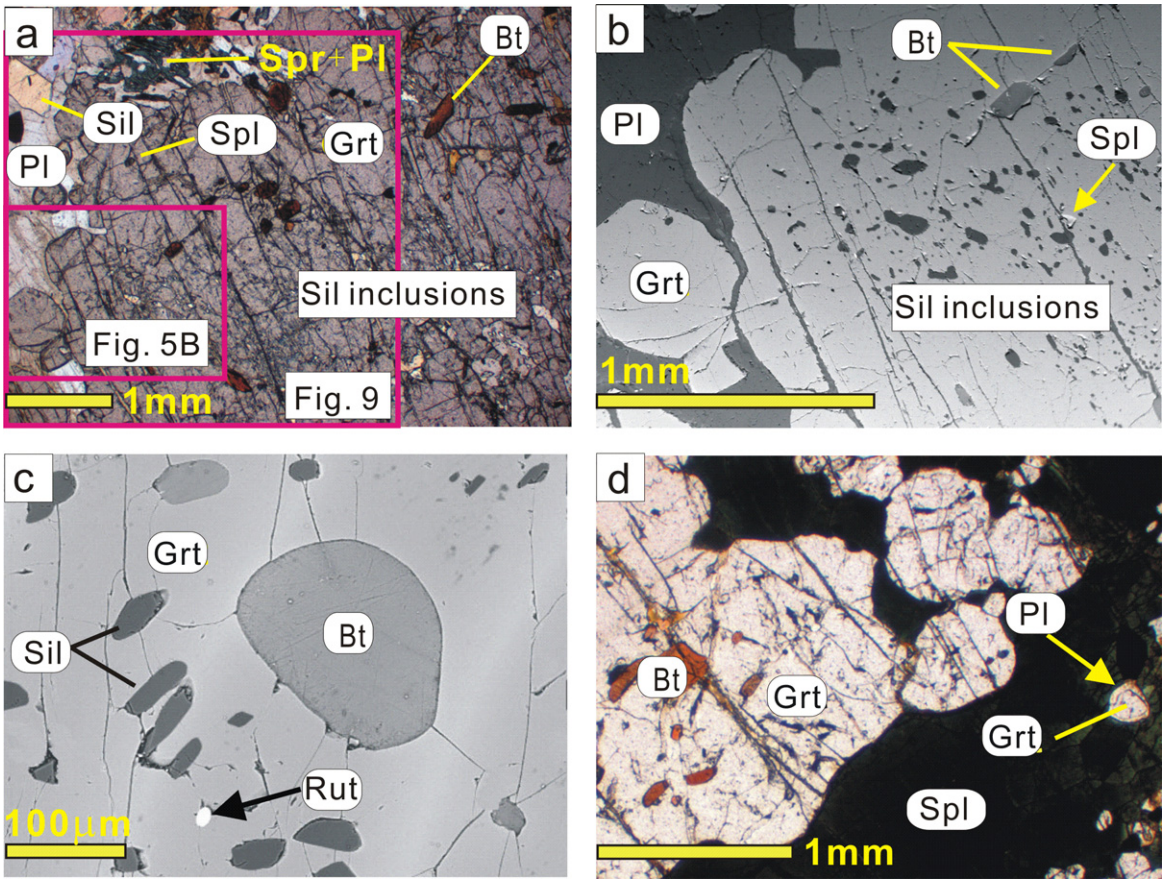

Fig. 5. Photomicrographs and BSE images of sapphirine granulites from the Daqingshan area. Mineral abbreviations are after Kretz (1983). (a) Photomicrograph showing inclusions of spinel, sillimanite, biotite and plagioclase in the core of a garnet porphyroblast in sample DP16 (Note: outlined are garnet areas shown in Figs. 5B and 9); (b) BSE image showing the same garnet porphyroblast as in Fig. 5a with an inclusion-free rim and a core containing many inclusions of sillimanite (black) and single euhedral inclusions of biotite and spinel (sample DP16); (c) BSE image of a garnet core with many inclusions of sillimanite, rutile and biotite. Sample DP21; (d) photomicrograph of a spinel–garnet granulite showing (sample DP 47). All scale bars are 1 mm.

4.4. Spinel + plagioclase symplectite (M_3)

In the sapphirine granulites fine-grained spinel + plagioclase symplectites (1) replace sapphirine + plagioclase symplectites (Fig. 7a), (2) develop around garnets (Fig. 7b), (3) form next to matrix-type sapphirines (Fig. 7c–d). The above textures (1) suggest that the spinel + plagioclase symplectites developed later than the sapphirine + plagioclase symplectites. This conclusion is also consistent with the reaction textures of Fig. 7c–d, which suggest that the spinel + plagioclase symplectites formed by the consumption of sapphirine. In addition, most of the spinel + plagioclase symplectites formed by the breakup of garnet (Fig. 7b).

Associated with the formation of the spinel + plagioclase symplectite are minor cordierite and corundum; the former mainly occurs along cracks in garnet (Fig. 7e), whereas the latter occur as tiny grains coexisting with cordierite in the spinel + plagioclase symplectites (Fig. 7d).

4.5. Retrogressive biotite + rutile + ilmenite (M_4)

Retrogressive biotite occurs as small flakes on the margins of garnet (Fig. 7b) or along cracks in garnet. Chemically, the retrogressive biotite possesses lower Ti contents than the matrix-type biotite. In addition, some high Ti biotite was transformed into Ti low biotite and vermicular or acicular rutile (Fig. 7e–f) or ilmenite; we suggest this reaction occurred synchronously with small biotite flakes at the start of the M_4 stage.

5. Mineral chemistry

All mineral analyses were made with an electron microprobe (Cameca SX50) housed at the Institute of Geology and Geophysics, Chinese Academy of Sciences in Beijing. Operating conditions were 15 kV and 15 nA with a point beam. Count times were 20 s on peaks, and 10 s on each background. Natural and synthetic phases were used as standards. The data were processed with an online ZAF-type correction. Representative mineral analyses of garnet, sapphirine and biotite are listed in Tables 1–3, and spinel, plagioclase and cordierite in Supplementary Tables 1–3. Structural formulae are given for fixed oxygen values and with Fe^{3+} calculated by stoichiometric charge balance.

5.1. Garnet

All garnet analyses are plotted in the grossular + spessartine–almandine–pyrope triangular diagram (Fig. 8). Garnet in the sapphirine granulites consists essentially of almandine (44–62%) and pyrope (35–53%), with minor grossular (2.4–3.7%) and spessartine (<1%) components (Table 1). All analyzed garnet cores and mantles have very limited compositional variations, but the rims show a remarkable drop in X_{Mg} and an increase in X_{Fe}. In view of the fact that the minerals enclosed in the garnet cores define the inclusion assemblage (M_0), it is important to understand the detailed compositional variations of these garnets. Compositional mapping for Mg, Fe, and Ca (Fig. 9a–c) was made for

Please cite this article in press as: Guo, J., et al., UHT sapphirine granulite metamorphism at 1.93–1.92 Ga caused by gabbronorite intrusions: Implications for tectonic evolution of the northern margin of the North China Craton. Precambrian Res. (2011), doi:10.1016/j.precamres.2011.07.020

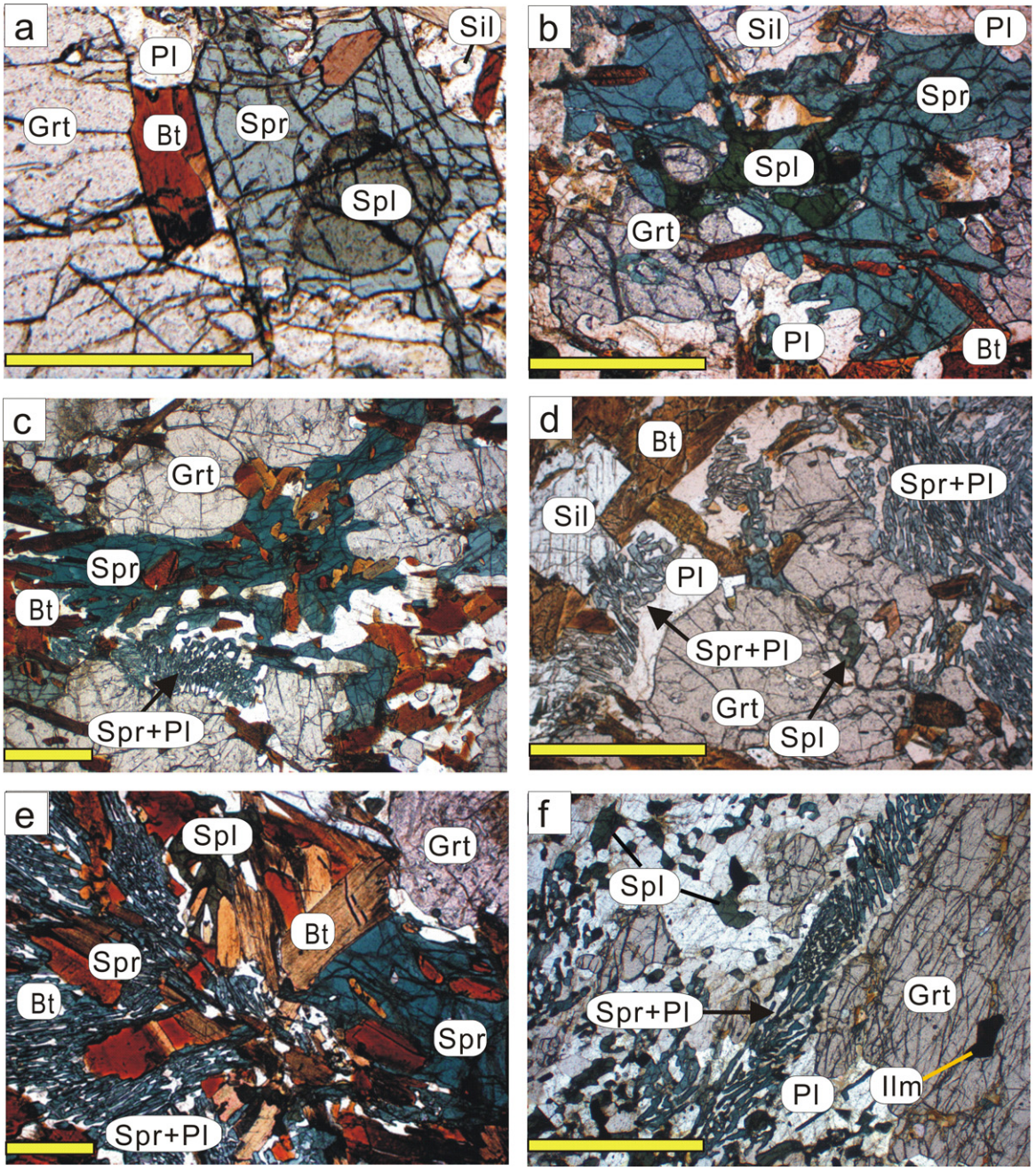

Fig. 6. Photomicrographs of the matrix assemblage in sapphirine granulites from the Daqingshan area. (a) Matrix-type sapphirine, biotite, sillimanite and garnet in sample DP15, in which the sapphirine encloses a spinel grain; (b) a large sapphirine grain encloses small grains of garnet and spinel. Sample DP17; (c) matrix-type sapphirine and symplectitic sapphirine + plagioclase in DP25. (d) Sapphirine + plagioclase symplectite growing between garnet and sillimanite in sample 17, (e) sapphirine + plagioclase symplectite around biotite in sample DP25, and (f) sapphirine + plagioclase symplectite as an isolated narrow band in sample DP18. All scale bars are 1 mm.

the garnet porphyroblasts, as shown in Fig. 5a. The results confirm that the garnets are nearly homogenous except for the outermost rims, which is attributed to the ambient high metamorphic temperature.

5.2. Sapphirine

All sapphirines are markedly high in Mg (X_{Mg} = 0.75–0.79) and Al (Al = 8.57–9.00 pfu) (Table 2, Fig. 10). Although the compositions of the sapphirines have considerable scatter, the molecular proportions of Al + Cr + Fe^{3+} vs. Si + Ti (Fig. 10) reveal an ideal Tschermak substitution of 2(Al + Cr + Fe^{3+}) = R^{2+} + Si in the sapphirines. The calculated $Fe^{3+}/(Fe^{2+} + Fe^{3+})$ ratios are lower than 0.30 (0.14–0.32, with 0.23 on average).

In general, symplectitic sapphirines are more peraluminous and magnesium than matrix sapphirines (Fig. 10). Also, the matrix sapphirines are slightly richer in Si than the symplectitic sapphirines. A sharp change in Al contents implies that the sapphirine-producing reactions for the matrix and symplectite types are different. Taking into account the textural relations described in the above section, we deduce that the growth of sympletitic sapphirine consumed more sillimanite but less garnet and spinel than did the matrix sapphirine. In addition, symplectitic sapphirine within sillimanite has the highest Al content up to 9.00 pfu.

Please cite this article in press as: Guo, J., et al., UHT sapphirine granulite metamorphism at 1.93–1.92 Ga caused by gabbronorite intrusions: Implications for tectonic evolution of the northern margin of the North China Craton. Precambrian Res. (2011), doi:10.1016/j.precamres.2011.07.020

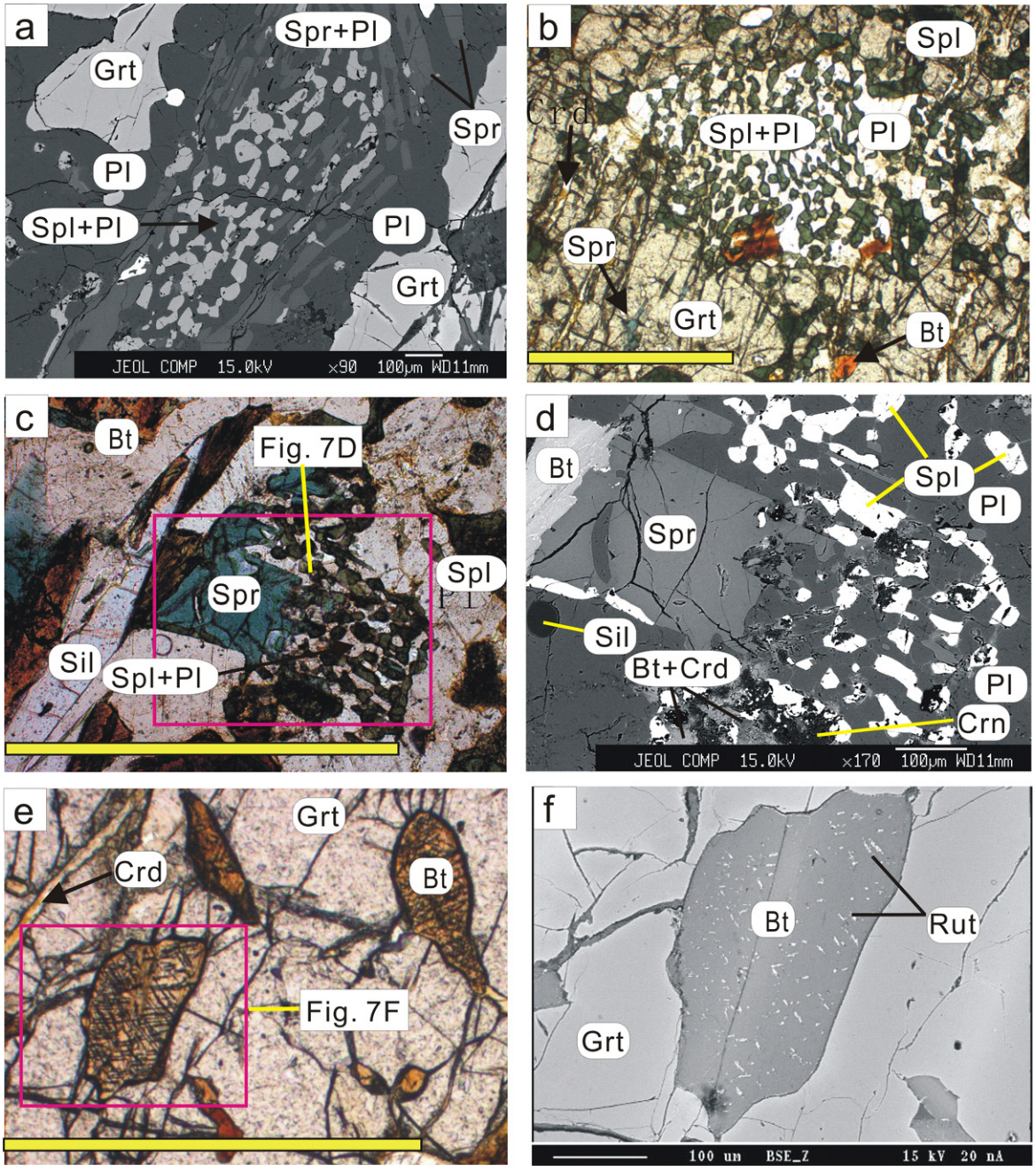

Fig. 7. (a) A BSE image showing a spinel + plagioclase symplectite replacing a sapphirine + plagioclase symplectite in sample DP18; (b) a photomicrograph showing a spinel + plagioclase symplectite replacing garnet in sample DP15; (c) a photomicrograph showing a spinel + plagioclase symplectite next to a matrix-type sapphirine in sample DP25. Position of Fig. 7D marked; (d) a BSE image showing an enlarged detail of the texture seen in Fig. 7C; (e) a photomicrograph showing rutile exsolution in titaniferous biotite inclusions in garnet in sample DP21. Position of Fig. 7F marked; (f) a BSE image showing an enlargement of the rutile exsolution in biotite seen in Fig. 8E. All scale bars are 1 mm.

5.3. Biotite

All biotites are essentially phlogopite-rich with Mg/(Mg + Fe) ratios of 0.67–0.84 (mostly 0.7–0.8) and an average of 0.75 (Table 3). The Mg/(Mg + Fe) ratios and X_{Mg} and X_{Fe} [=Fe/(Mg + Fe + Mn)] values of biotites vary over a small range regardless of their different textural types (Fig. 11a).

In the sapphirine granulites, the large matrix-type biotites without rutile and ilmenite exsolutions usually have Ti contents over 5 wt.%, and the inclusion-type biotites within sapphirine have even higher TiO_2 up to 6.3 wt.% (Table 3). Comparatively, the retrogressive biotites and those with rutile and ilmenite exsolutions have low Ti contents. Titaniferous biotites also occur in the spinel–garnet granulite and the host gneiss, with their highest Ti content even reaching 7.7 wt.% and 7.6 wt.% respectively. In biotites from the sapphirine granulite and the host gneiss, Ti and Al(VI) vary inversely implying that the Ti substitutes for Al(VI) on an approximate 1:1 basis (Fig. 11b). But the biotites from the spinel–garnet granulite are slightly off the Ti and Al(VI) substitution line with a 45° slope (Fig. 11b).

In general, Ti concentration in biotite increases as a function of temperature in a non-linear fashion (Henry et al., 2005; Cesare et al., 2008); a high Ti content in biotite is attributed to high-temperature. For comparison, we use an empirical model for solution of Ti in

Please cite this article in press as: Guo, J., et al., UHT sapphirine granulite metamorphism at 1.93–1.92 Ga caused by gabbronorite intrusions: Implications for tectonic evolution of the northern margin of the North China Craton. Precambrian Res. (2011), doi:10.1016/j.precamres.2011.07.020

Table 1
Representative analyses of garnets from sapphirine granulites.

Sample no.	DP17	DP17	DP18	DP25	DP25	DP42	DP42	DP42	DP45	DP45	DP45	DP46
Analysis no.	2–4	1–102	1–89	4–23	4–22	2–23	2–34	2–17	1–8	1–7	1–6	1–68
Remarks	Core	Rim	Rim	Core	Rim	Core	Mantle	Rim	Core	Mantle	Rim	Rim
SiO_2	37.78	39.60	39.87	39.81	39.43	37.15	37.31	39.81	39.29	39.33	39.42	39.10
TiO_2	0.05	0.04	0.02	0.06	0.08	0.00	0.02	0.00	0.07	0.05	0.04	0.05
Al_2O_3	22.46	22.20	22.12	22.85	22.73	22.59	22.41	22.35	22.57	22.47	22.23	22.10
Cr_2O_3	0.04	0.00	0.02	0.02	0.01	0.01	0.02	0.00	0.00	0.00	0.00	0.00
FeO	27.74	25.50	26.44	26.22	26.39	29.87	27.34	25.81	26.10	27.01	29.17	27.70
MnO	0.33	0.30	0.41	0.31	0.30	0.37	0.37	0.27	0.28	0.29	0.39	0.28
MgO	11.59	11.29	10.99	11.71	11.55	10.49	11.26	11.55	11.44	10.92	9.15	10.12
CaO	0.81	1.07	0.89	0.80	0.81	0.86	1.13	1.05	0.92	0.91	0.99	0.98
Na_2O	0.00	0.01	0.01	0.01	0.03	0.01	0.00	0.00	0.09	0.09	0.10	0.00
Total	100.80	100.01	100.76	101.78	101.32	101.36	99.86	100.84	100.75	101.07	101.49	100.32
Si^{IV}	2.853	3.007	3.016	2.968	2.956	2.814	2.845	2.997	2.96	2.965	2.996	2.987
Al^{IV}	0.147	0	0	0.032	0.044	0.186	0.155	0.003	0.04	0.035	0.004	0.013
Al^{VI}	1.851	1.985	1.97	1.975	1.962	1.829	1.857	1.977	1.963	1.961	1.987	1.976
Ti	0.003	0.002	0.001	0.003	0.004	0	0.001	0	0.004	0.003	0.002	0.003
Cr	0.003	0	0.001	0.001	0	0.001	0.001	0	0	0	0	0
Fe^{2+}	1.752	1.619	1.673	1.635	1.655	1.892	1.744	1.625	1.644	1.703	1.854	1.77
Mg	1.305	1.278	1.239	1.301	1.291	1.184	1.28	1.296	1.284	1.227	1.036	1.153
Mn	0.021	0.019	0.026	0.02	0.019	0.024	0.024	0.017	0.018	0.019	0.025	0.018
Ca	0.065	0.087	0.072	0.064	0.065	0.07	0.092	0.084	0.074	0.074	0.081	0.08
Na	0	0.002	0.001	0.001	0.004	0.001	0	0	0.013	0.013	0.015	0
Alm	43.575	53.53	54.806	43.965	44.286	47.728	43.703	53.001	44.136	45.854	61.793	58.107
Pyrope	52.909	42.887	41.872	52.645	52.316	48.451	51.595	43.58	52.145	50.356	34.68	38.607
Gross	2.495	2.932	2.37	2.506	2.613	2.798	3.659	2.839	3.002	3.02	2.698	2.684
Spess	0.861	0.652	0.885	0.797	0.767	0.971	0.974	0.581	0.718	0.77	0.829	0.596
Uvaro	0.16	0	0.067	0.086	0.018	0.051	0.069	0	0	0	0	0.006

Note: (1) cations to 12 oxygens; (2) all Fe is assumed to be Fe^{2+}.

biotites with variation in temperature (Fig. 11c; Patiño Douce, 1993). Surprisingly, the Ti contents (up to 0.42 pfu) of some biotites are much higher than the highest value of 0.35 pfu (Fig. 11a–b) obtained by the synthesis experiments, which corresponds to a temperature of ~950 °C. It is important to note that the Ti solubility in biotite increases with temperature in a robust non-linear fashion (Fig. 11c; Patiño Douce, 1993 and references therein), although the actual Ti content may also be affected by other factors such as oxygen fugacity. Accordingly, the very high Ti contents (up to 0.42 pfu) of the biotites, together with their high X_{Mg} and low Al(VI), should document an ultrahigh metamorphic temperature of >950 °C.

5.4. Spinel

All spinels are Fe-rich (X_{Mg} = 0.29–0.52) and contain high contents of hercynite (Supplementary Table 1), with a $Fe^{3+}/(Fe^{2+} + Fe^{3+})$ ratio varying from 0.02 to 0.12, indicating a low Fe^{3+} content. Both Cr and Ti contents are very much lower. Usually, spinel in the matrix has a slightly high X_{Mg} [=Mg/(Mg + Fe)] because of very tiny (<1 μm) magnetite exsolutions, while symplectitic spinel has relatively wide X_{Mg} variations.

5.5. Plagioclase

All major textural types of plagioclase, including inclusions within garnet, as granular matrix grains, coronae around garnets, long lamellae in symplectites with sapphirine, and fine-grained plagioclase in symplectites with spinel are Ab-rich with 23–40% An (Supplementary Table 2). In general, inclusion-type plagioclase in garnet has the lowest An component (e.g. 26%), while the granular matrix-type plagioclase has the highest An component (e.g. 40%).

5.6. Cordierite

Anhedral cordierite occurs in cracks in some garnet porphyroblasts, where it is associated with spinel + plagioclase symplectites. All analyzed cordierites are Mg-rich, with Mg/(Mg + Fe^{2+}) ratios between 0.87 and 0.88 (Supplementary Table 3).

5.7. Perthite/mesoperthite

Perthite/mesoperthite is not present in the sapphirine granulite, but is present in its host rock – the quartzo-feldspathic gneiss. This perthite/mesoperthite has regular, coarse and continuous lamellae, which are generally interpreted as evidence for slow cooling after peak UHT metamorphism (e.g., Hayob et al., 1989). A number of examples have shown that the compositions of perthite from UHT rocks can be used to estimate the minimum peak temperature of UHT metamorphism using ternary-feldspar geothermometers (e.g. Hokada, 2001; Hokada and Suzuki, 2006; Prakash et al., 2006; Santosh et al., 2007a; Pilugin et al., 2009).

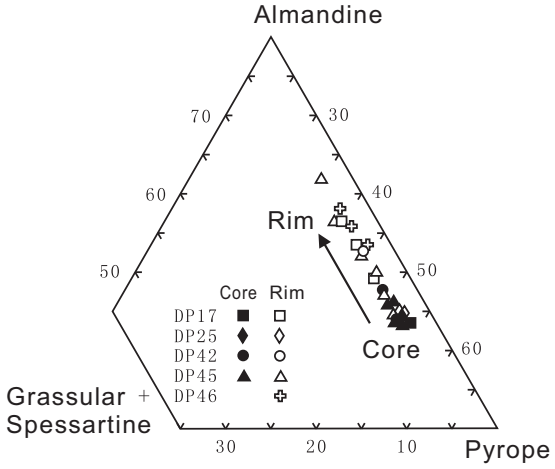

Fig. 8. Plot of garnet compositions in grossular + spessartine–almandine–pyrope triangular space, showing the core-to-rim variations of Ca, Mn, Fe and Mg in five samples.

Table 2
Representative analyses of sapphirines from sapphirine granulites.

Sample no.	DP17	DP17	DP17	DP18	DP18	DP25	DP25	DP25	DP25	DP42	DP42	DP45	DP45	DP45	DP45	DP46
Analysis no.	1–108	2–8	2–10	1–99	1–91	4–11	4–21	4–15	3–74	2–24	2–33	1–58	1–62	1–54	1–44	1–64
Remarks	Core	Sym.grt	Sym.sil	Rim	Sym.spl	Core	Core	Sym.grt	Sym.bt	Sym.sil	Sym.grt	Core	In grt	Sym.spl	Sym.grt	Sym.grt
SiO_2	12.94	11.96	11.88	12.53	12.18	12.47	12.30	11.78	11.90	10.95	12.04	13.42	12.93	11.76	12.02	12.25
TiO_2	0.07	0.08	0.05	0.01	0.00	0.10	0.09	0.03	0.08	0.12	0.05	0.14	0.14	0.04	0.12	0.06
Al_2O_3	60.39	62.47	63.20	62.26	62.63	60.83	61.54	63.29	63.40	63.62	62.98	60.21	61.68	62.41	62.69	62.29
Cr_2O_3	0.09	0.02	0.07	0.05	0.10	0.06	0.07	0.07	0.15	0.13	0.09	0.06	0.11	0.11	0.08	0.08
FeO	11.17	10.48	10.11	10.17	10.24	11.72	11.37	9.92	10.11	10.58	9.48	11.02	10.06	9.73	9.94	9.69
MnO	0.02	0.05	0.09	0.00	0.02	0.00	0.04	0.01	0.02	0.03	0.00	0.00	0.02	0.01	0.02	0.02
MgO	14.74	14.81	14.72	14.66	14.86	14.63	14.59	14.81	14.75	14.49	15.34	14.90	15.24	14.82	14.95	15.02
CaO	0.04	0.03	0.05	0.00	0.05	0.02	0.01	0.01	0.03	0.02	0.03	0.03	0.02	0.02	0.00	0.00
Na_2O	0.01	0.01	0.00	0.00	0.00	0.00	0.01	0.00	0.01	0.02	0.00	0.00	0.00	0.00	0.01	0.00
K_2O	0.00	0.00	0.00	0.00	0.01	0.00	0.00	0.00	0.02	0.00	0.00	0.00	0.01	0.02	0.00	0.02
Total	99.46	99.90	100.16	99.68	100.08	99.82	100.01	99.91	100.47	99.96	100.01	99.76	100.21	98.91	99.83	99.44
Si	1.566	1.436	1.422	1.508	1.459	1.505	1.48	1.411	1.419	1.314	1.438	1.619	1.547	1.423	1.442	1.475
Ti	0.006	0.007	0.004	0.001	0	0.009	0.008	0.002	0.007	0.011	0.004	0.012	0.012	0.003	0.011	0.005
Al	8.619	8.842	8.915	8.832	8.844	8.66	8.735	8.94	8.917	8.999	8.868	8.567	8.7	8.901	8.866	8.838
Cr	0.008	0.002	0.007	0.005	0.009	0.006	0.007	0.007	0.014	0.012	0.009	0.005	0.011	0.011	0.007	0.008
Fe^{3+}	0.231	0.272	0.225	0.143	0.23	0.305	0.284	0.226	0.22	0.344	0.239	0.164	0.171	0.239	0.223	0.198
Fe^{2+}	0.9	0.78	0.786	0.88	0.795	0.878	0.86	0.768	0.789	0.718	0.708	0.949	0.835	0.746	0.774	0.777
Mn	0.002	0.005	0.009	0	0.002	0	0.004	0.001	0.002	0.003	0	0	0.002	0.001	0.002	0.002
Mg	2.659	2.65	2.625	2.632	2.653	2.632	2.618	2.644	2.623	2.591	2.73	2.679	2.718	2.671	2.673	2.693
Ca	0.006	0.003	0.007	0	0.006	0.003	0.001	0.001	0.004	0.003	0.004	0.004	0.002	0.002	0	0
Na	0.003	0.002	0	0	0	0	0.003	0	0.001	0.005	0	0	0	0	0.003	0
K	0	0	0	0	0.002	0	0	0	0.003	0	0	0	0.001	0.003	0	0.004
Total	14	13.999	14	14.001	14	13.998	14	14	13.999	14	14	13.999	13.999	14	14.001	14
$Mg/(Mg + Fe^{2+})$	0.75	0.77	0.77	0.75	0.77	0.75	0.75	0.77	0.77	0.78	0.79	0.74	0.76	0.78	0.78	0.78
$Fe^{3+}/(Fe^{2+} + Fe^{3+})$	0.20	0.26	0.22	0.14	0.22	0.26	0.25	0.23	0.22	0.32	0.25	0.15	0.17	0.24	0.22	0.20

Notes: (1) cations to 20 oxygens. (2) Core = core of coarse-grained sapphirine; rim = rim of coarse-grained sapphirine. (3) Sapphirines abbreviated as sym.grt, sym sil, sym.spl, sym.bt are those in the symplectite with plagioclase close to garnet, sillimanite, spinel, biotite, respectively. (4) Fe^{2+} and Fe^{3+} are calculated by stoichiometric charge balance.

Please cite this article in press as: Guo, J., et al., UHT sapphirine granulite metamorphism at 1.93–1.92 Ga caused by gabbronorite intrusions: Implications for tectonic evolution of the northern margin of the North China Craton. Precambrian Res. (2011), doi:10.1016/j.precamres.2011.07.020

Table 3
Representative analyses of biotites.

Sample no.	DP17	DP17	DP25	DP25	DP25	DP25	DP45	DP45	DP45	DP45	DP21	DP21	DP21	DP17	DQ17	DQ17
Analysis no.	2–16	2–11	4–3	3–73	4–9	3–72	1–33	1–21	1–11	1–17	1–84	1–86	1–72	4–54	3–10	3–22
Remarks	In grt	In grt	In grt	Granular	In spr	Retro	In grt	In spr	Retro	Retro	In grt	In grt	Ex.rut	In grt	In grt	In pl
SiO_2	38.02	38.18	36.69	36.70	36.62	37.76	37.09	37.43	39.94	40.09	37.91	38.18	38.23	36.34	37.35	36.63
TiO_2	4.80	2.67	6.20	4.14	6.32	1.65	5.74	5.13	1.54	2.42	7.43	7.73	2.20	7.15	7.59	7.37
Al_2O_3	17.65	17.75	15.69	16.14	15.19	17.65	15.74	16.02	15.82	16.27	16.35	16.16	17.17	16.80	14.68	14.69
Cr_2O_3	0.02	0.02	0.06	0.18	0.09	0.03	0.04	0.00	0.09	0.02	0.00	0.00	0.01	0.05	0.10	0.20
FeO	8.00	10.53	11.59	11.00	12.72	9.55	9.18	9.07	7.11	7.98	9.73	7.34	9.31	9.78	11.32	15.02
MnO	0.00	0.00	0.00	0.00	0.00	0.00	0.00	0.04	0.00	0.04	0.01	0.00	0.00	0.00	0.00	0.01
MgO	18.12	17.14	15.58	15.94	14.56	18.33	18.16	17.99	21.03	20.26	15.90	17.36	18.12	15.69	14.81	12.26
CaO	0.00	0.01	0.00	0.03	0.03	0.02	0.00	0.03	0.05	0.01	0.00	0.00	0.04	0.00	0.00	0.00
Na_2O	0.13	0.25	0.12	0.21	0.41	0.49	0.28	0.28	0.36	0.35	0.29	0.21	0.24	0.37	0.10	0.05
K_2O	9.69	9.42	9.59	9.67	8.76	8.73	9.36	9.39	8.25	7.29	8.66	8.78	8.80	9.22	9.52	9.47
Total	96.43	95.97	95.53	94.01	94.70	94.21	95.60	95.39	94.17	94.71	96.26	95.76	94.10	95.41	95.47	95.69
Si	2.71	2.76	2.70	2.73	2.72	2.76	2.69	2.72	2.87	2.85	2.72	2.72	2.79	2.65	2.74	2.73
Al^{IV}	1.29	1.24	1.30	1.27	1.28	1.24	1.31	1.28	1.13	1.15	1.28	1.28	1.21	1.35	1.26	1.27
Ti	0.26	0.14	0.34	0.23	0.35	0.09	0.31	0.28	0.08	0.13	0.40	0.41	0.12	0.39	0.42	0.41
Al^{VI}	0.19	0.27	0.06	0.15	0.05	0.28	0.03	0.09	0.21	0.22	0.10	0.08	0.26	0.09	0.01	0.02
Cr	0.00	0.00	0.00	0.01	0.01	0.00	0.00	0.00	0.01	0.00	0.00	0.00	0.00	0.00	0.01	0.01
Fe^{2+}	0.48	0.64	0.71	0.68	0.79	0.58	0.56	0.55	0.43	0.47	0.58	0.44	0.57	0.60	0.69	0.94
Mn	0.00	0.00	0.00	0.00	0.00	0.00	0.00	0.00	0.00	0.00	0.00	0.00	0.00	0.00	0.00	0.00
Mg	1.92	1.84	1.71	1.77	1.61	2.00	1.96	1.95	2.25	2.15	1.70	1.84	1.97	1.70	1.62	1.36
Ca	0.00	0.00	0.00	0.00	0.00	0.00	0.00	0.00	0.00	0.00	0.00	0.00	0.00	0.00	0.00	0.00
Na	0.02	0.04	0.02	0.03	0.06	0.07	0.04	0.04	0.05	0.05	0.04	0.03	0.03	0.05	0.01	0.01
K	0.88	0.87	0.90	0.92	0.83	0.81	0.87	0.87	0.76	0.66	0.79	0.80	0.82	0.86	0.89	0.90
Total	7.74	7.79	7.74	7.80	7.70	7.83	7.78	7.77	7.78	7.69	7.61	7.60	7.78	7.69	7.66	7.66
$Mg/(Mg+Fe^{2+})$	0.80	0.74	0.71	0.72	0.67	0.77	0.78	0.78	0.84	0.82	0.74	0.81	0.78	0.74	0.70	0.59

Notes: (1) cations to 11 oxygens. (2) Sample DP21 is a spinel garnetite, sample DQ17 is an orthopyroxene–garnet–biotite–plagioclase gneiss, all other samples are sapphirine granulites. (3) Retro = retrograde small biotite flake, ex.ru = biotite with rutile exsolution. (4) All Fe is assumed to be Fe^{2+}.

Please cite this article in press as: Guo, J., et al., UHT sapphirine granulite metamorphism at 1.93–1.92 Ga caused by gabbronorite intrusions: Implications for tectonic evolution of the northern margin of the North China Craton. Precambrian Res. (2011), doi:10.1016/j.precamres.2011.07.020

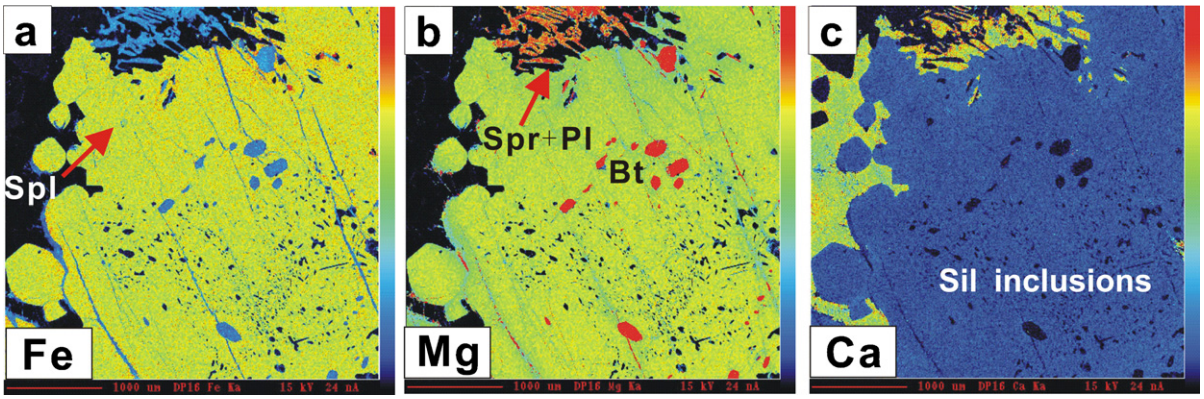

Fig. 9. X-ray maps of Fe, Mg and Ca in a garnet porphyroblast seen in Fig. 5a, showing variations from core to rim. The maps indicate that the garnet contains (a) spinel inclusions, (b) biotite inclusions (also shown is an adjacent symplectite of sapphirine + plagioclase), and (c) inclusions of sillimanite.

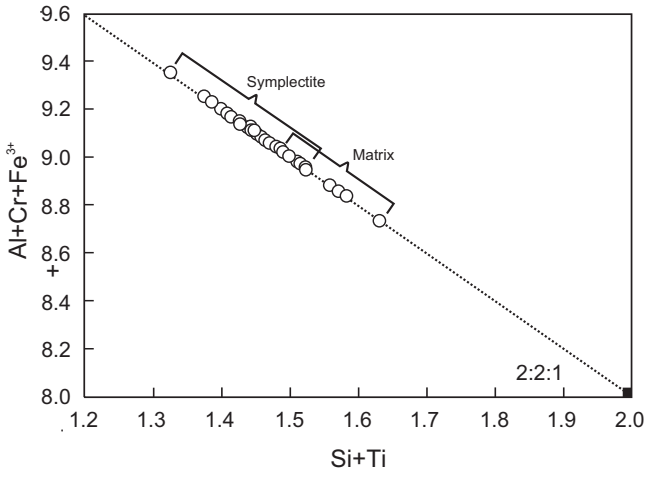

Fig. 10. Molecular proportions of Al + Cr + Fe^{3+} vs. Si + Ti (per 20 oxygen formula unit) for sapphirine. Diagonal line represents the ideal tschermak substitution from the 2:2:1 to the 7:9:3 end-member compositions.

Fig. 12 shows that temperatures estimated from the compositions of mesoperthites from the quartzo-feldspathic gneiss (host rocks of the sapphirine granulite) in the Dongpo area range between 900 °C and 950 °C, further supporting the ultrahigh-temperature metamorphism.

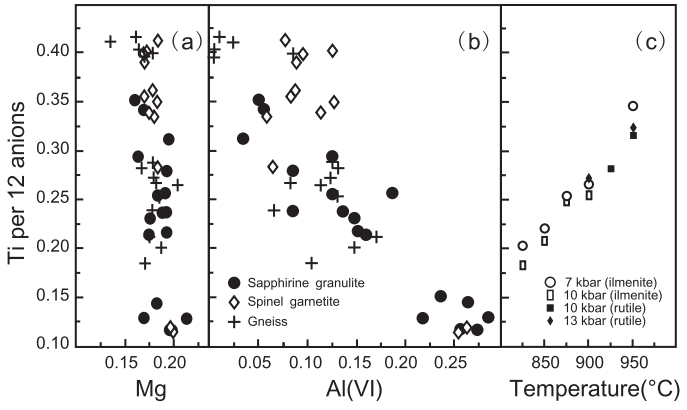

Fig. 11. Plots of biotite compositions showing correlations between Ti and Mg (a), and between Ti and Al (b). (c) Shows temperature variation vs. Ti content in experimental biotites associated with Ti-saturating phases such as rutile and ilmenite, indicating that the Ti solubility in biotite increases with temperature up to ~950 °C (Patiño Douce, 1993).

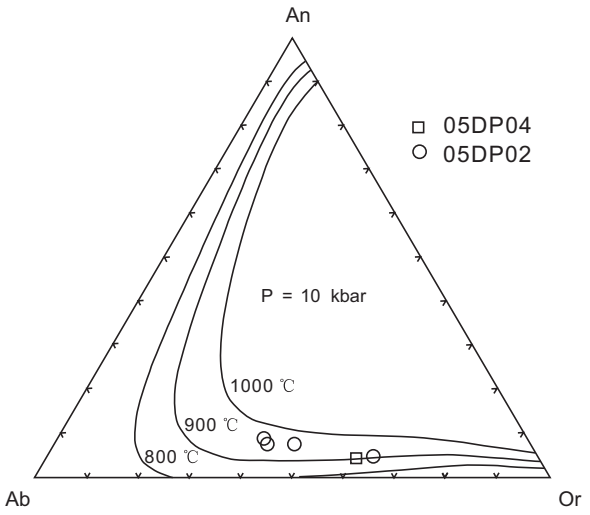

Fig. 12. An Ab–An–Or diagram with temperature estimates (UHT of >900 °C) based on the compositions of perthites/mesoperthites from the two samples of quartzo-feldspathic gneiss – the host rock of the sapphirine granulites. Temperature isotherms are for 10 kbar, from Fuhrman and Lindsley (1988).

6. Metamorphic reactions, phase equilibrium calculations and *P–T* path

6.1. Metamorphic reactions

6.1.1. Development of the matrix assemblage (M_1)

The major phase change from the mineral inclusion assemblage (M_0) to the matrix assemblage (M_1) is characterized by the appearance of sapphirine. Using the SiO_2–Al_2O_3–(FeO + MgO) diagrams (Fig. 13) for the inclusion and matrix mineral assemblages, the growth of sapphirine mainly consumed garnet, spinel and sillimanite; no quartz was involved. Accordingly, the major sapphirine-producing reaction can be illustrated as follows:

$$\begin{aligned}&\text{Pyrope/Almandine} + \text{Spinel} + \text{Sillimanite} \rightarrow \text{Sapphirine}\\&(\text{Mg, Fe})_3\text{Al}_2\text{Si}_3\text{O}_{12} + (\text{Mg, Fe})\text{Al}_2\text{O}_4 + \text{Al}_2\text{SiO}_5\\&\quad\rightarrow (\text{Mg, Fe})_{3.5}\text{Al}_9\text{Si}_{1.5}\text{O}_{20}\end{aligned} \quad (1)$$

Here, the formula of sapphirine was roughly determined from the average analyses listed in Table 3 regardless of the Fe^{3+}/Fe^{2+} ratios. When garnet decomposed, Ca released must have produced plagioclase, but in limited amounts, as implied by the presence of small plagioclase grains adjacent to garnet (Fig. 6a–c). In addition, biotite must have been involved in the reaction in order to maintain

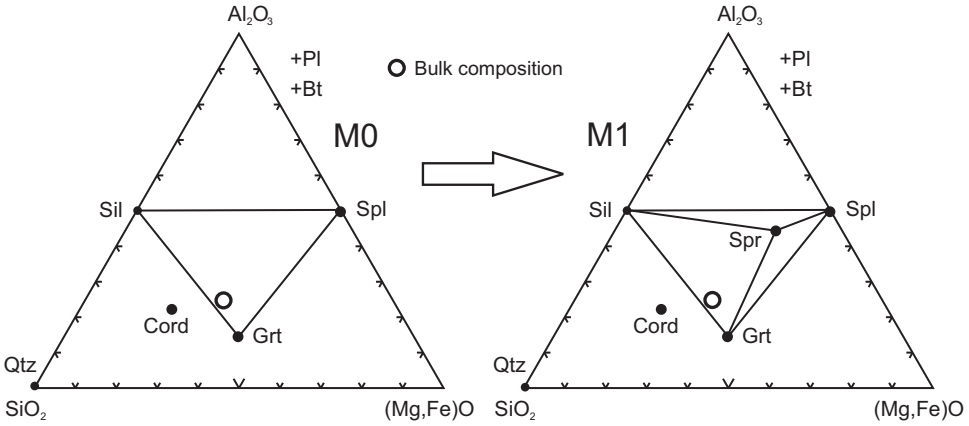

Fig. 13. SiO_2–Al_2O_3–(FeO + MgO) triangular diagrams showing compositions and mineral assemblages of sapphirine granulites – the inclusion assemblage (M_0) and the matrix assemblage (M_1). The equilibrium mineral assemblages are indicated by tie lines, and the bulk-rock compositions by circles. The arrows indicate the reaction trends from M_0 to M_1.

Mg–Fe equilibrium between the Mg and Fe minerals and to buffer the Ti components with rutile and ilmenite.

Furthermore, the protolith of the sapphirine granulite was most likely the restite of partially melted pelitic rocks, as indicated by the presence of coexisting quartz–plagioclase veins, which are up 10–20% of the outcrop (Fig. 4a–b). The removal of such melts would result in a drop in abundance of Si, Ca, and Na in the protolith.

6.1.2. Formation of the Spr–Pl symplectite (M_2)

For the sapphirine + plagioclase symplectites that occur between garnet and sillimanite (Fig. 6d), it is clear that the main reactant minerals were garnet and sillimanite without spinel. Thus, possible metamorphic reactions to form the sapphirine + plagioclase symplectites are combinations of the following:

$$\begin{aligned}&\text{Grossular} + 2\,\text{Sillimanite} + SiO_2 = 3\,\text{Anorthite}\\&Ca_3Al_2Si_3O_{12} + 2Al_2SiO_5 + SiO_2 = 3CaAl_2Si_2O_8\end{aligned} \quad (2)$$

and

$$\begin{aligned}&7\ \text{Pyrope/Almandine} + 20\,\text{Sillimanite} = 6\,\text{Sapphirine} + 32\,SiO_2\\&7(Mg,\ Fe)_3Al_2Si_3O_{12} + 20Al_2SiO_5 = 6(Mg,\ Fe)_{3.5}Al_9Si_{1.5}O_{20} + 32SiO_2\end{aligned} \quad (3)$$

The net reaction from the above two reactions is 32 grossular + 84 sillimanite + 7 pyrope/almandine = 96 anorthite + 6 sapphirine, which suggests that the volume ratio of plagioclase to sapphirine should be around 10:1, but the observed modal ratio of plagioclase to sapphirine in the rock is less than 5:1. This difference most likely resulted from the removal of silica by melts as indicated by the presence of quartz + plagioclase veins in the sapphirine granulite layer (Fig. 4a–b).

The above reactions also suggest that Ca in symplectitic plagioclase came from garnet. However, mineral chemistry shows that the Ca contents in symplectitic plagioclases close to garnet are even lower than those close to sillimanite, suggesting that the Ca contents released by the grossular breakdown are less than those of symplectitic plagioclase obtained externally from the matrix. Thus, the balance of the reaction pairs most likely shifted to reaction (3), releasing more SiO_2 than was absorbed by reaction (2).

In this case, there must have been another way of absorbing the excess quartz on account of the absence of quartz in the mineral assemblage. The optimal choice is the biotite breakdown reaction, which could be facilitated by quartz; such biotite breakdown textures widely are developed in the M_2 assemblage (Fig. 6e). The responsible reaction can be roughly expressed as follow:

$$\begin{aligned}&\text{Biotite} + \text{Plagioclase} + SiO_2 \rightarrow \text{Sapphirine}\\&+ \text{Plagioclase}\,(M_2,\ \text{Ca-rich}) + \text{melt}\end{aligned} \quad (4)$$

This reaction could result in the release of melts comprising K, Na, Al, Si, and H_2O components, and this is consistent with the presence of very small granite veins observed in the sapphirine granulite layer (Fig. 4).

6.1.3. Formation of the spinel + plagioclase symplectite (M_3)

Because most spinel + plagioclase symplectites occur around garnet or sillimanite (Fig. 7b), their formation should have involved the consumption of garnet by the following possible reaction:

$$\begin{aligned}&\text{Grossular} + \text{Pyrope} + \text{Sillimanite} = 3\,\text{Anorthite} + 3\,\text{Spinel}\\&Ca_3Al_2Si_3O_{12} + Mg_3Al_2Si_3O_{12} + Al_2SiO_5 = 3CaAl_2Si_2O_8 + 3MgAl_2O_4\end{aligned} \quad (5)$$

In addition, some spinel + plagioclase symplectites replace sapphirine + plagioclase (Fig. 7a) or occur around matrix-type sapphirine (Fig. 7c–d), suggesting that the symplectite formation consumed sapphirine. Moreover, some fine-grained cordierite and corundum formed in association with the sympectitic spinel, suggesting the following possible reaction:

$$\begin{aligned}&10\,\text{Sapphirine} = 29\,\text{Spinel} + 3\,\text{Cordierite} + 15\,\text{Corundum}\\&10(Mg,\ Fe)_{3.5}Al_9Si_{1.5}O_{20} = 29(Mg,\ Fe)Al_2O_4 + 3(Mg,\ Fe)_2Al_4Si_5O_{18} + 15Al_2O_3\end{aligned} \quad (6)$$

6.2. Phase equilibrium calculations

Mineral assemblages, metamorphic reactions and phase relations in the sapphirine granulites described above can be illustrated with the K_2O–Na_2O–CaO–FeO–MgO–Al_2O_3–SiO_2–H_2O [NCKFMASH] component system. The bulk-rock composition of sample DP25, in wt.%, is SiO_2 = 38.88, TiO_2 = 1.54, Al_2O_3 = 30.05, FeO_{tot} = 15.26, MnO = 0.12, MgO = 7.50, CaO = 1.83, Na_2O = 1.59, K_2O = 1.36, P_2O_5 = 0.06 and LOI (loss on ignition) = 0.57 (by standard wet chemical methods). This bulk-rock composition was corrected into the unit of mol% for the *P–T* pseudosection calculations in the NCKFMASH system (Fig. 14). SiO_2, Al_2O_3, FeO and MgO are the four major components with about 94% in mole contents, while CaO, Na_2O, K_2O and TiO_2 are minor components with about 6% in mole contents. Demonstrably, these rocks are not equivalent to Mg–Al granulites in bulk composition; they have very low SiO_2 (39 wt.%),

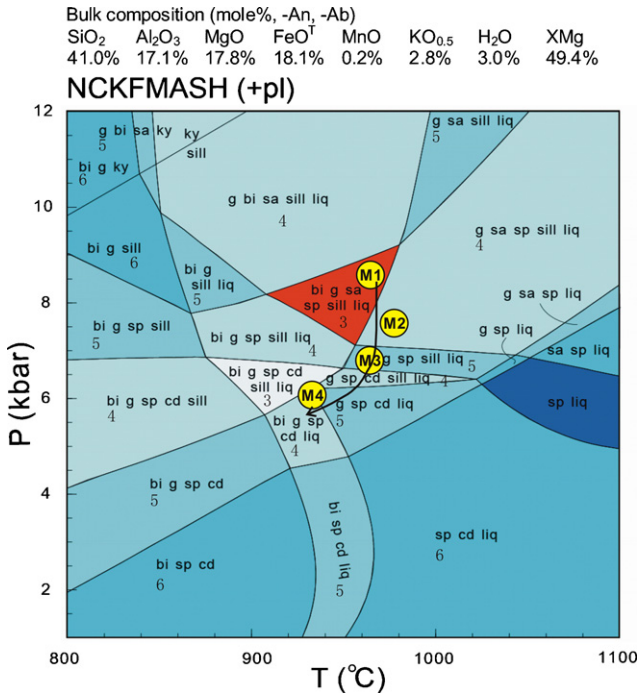

Fig. 14. A calculated *P–T* pseudosection and *P–T* path for sample DP25 for the given bulk composition in the NCKFMASH (+pl) system, labeled with mineral assemblage fields. Field variance is denoted by number. A low-variance (variance = 3) field right on the center coloured red with temperatures between about 910 °C and 980 °C corresponds closely to the matrix assemblage (M_1), indicating ultrahigh-temperature metamorphism. The transition from the matrix assemblage (M_1) to the sapphirine + plagioclase symplectite assemblage (M_2) can be symbolized by the biotite breakdown reaction, which indicates decompression. The transition from the sapphirine + plagioclase symplectite (M_2) to the spinel + plagioclase ± cordierite ± corundum assemblage (M_3) is indicated by the breakdown of sapphirine and the formation of cordierite, both of which are typical results of decompression. Subsequently, the appearance of retrogressive biotite (M_4) indicates cooling. Accordingly, a *P–T* path can be defined starting from the peak UHT (910–980 °C) metamorphism (M_1) followed by near-isothermal decompression (M_2 and M_3), and by decompressional cooling (M_4), based on the change in mineral assemblages in sapphirine granulites from the Daqingshan area. (For interpretation of the references to color in this figure legend, the reader is referred to the web version of the article.)

high Al contents, and X_{Mg} as low as about 0.5, which can account for the absence of orthopyroxene in the peak mineral assemblage. Because quartz is absent in the rocks and only a small amount of corundum appears in the M_3 assemblage as the product of sapphirine or spinel breakdown, the NCKFMASH system chosen for this study is a quartz–corundum-absent system.

For an Al-rich and silica-undersaturated system, it is not easy to elucidate the high- to ultrahigh-temperature *P–T* conditions on account of the lack of experimental constraints on phase relationships (Harley, 1998c; Kelsey et al., 2005 and references therein). Nevertheless, an alternative is produced by thermodynamic calculations, the best choice of which is the THERMOCALC program (Powell et al., 1998) with which it is possible to calculate phase equilibrium applicable to silica-undersaturated granulite facies meta-pelitic compositions for both quartz–corundum-absent and corundum-bearing assemblages, using the activity–composition model for sapphirine (Kelsey et al., 2004, 2005). However, it must be noted that this approach relies heavily on the adopted activity–composition models, some of which are untested against experimental data in the NCKFMASH system, and thus the results of the THERMOCALC calculations must be treated as exploratory and semi-quantitative.

Here, we calculate phase equilibrium for the matrix mineral assemblage (M1) of the sapphirine granulite using THERMOCALC v 3.23 (Powell et al., 1998), with the internally consistent data-set 5.5 of Holland and Powell (1998) (27 January 2004 update). The thermodynamic data and data-file scripts for sapphirine are taken from Kelsey et al. (2004, 2005), and Fe^{3+} was not incorporated. The bulk composition analysis of sample DP25 is used for the calculation on the assumption that with this composition the matrix mineral assemblage reached complete equilibrium during the peak metamorphism. A granitic melt is assumed to exist with the matrix assemblage during the peak metamorphism, but it was expelled later. Then, assuming plagioclase was an excess phase in all the fields, we calculated a *P–T* pseudosection for sapphirine granulite sample DP25, and the result is presented in Fig. 14.

In the calculated *PT* pseudosection (Fig. 14), two lowest variance (variance = 3) fields are in the center of the figure. On the high-pressure and high-temperature side is a triangular field labeled M_2, denoting the matrix assemblage of garnet + sapphirine + sillimanite + spinel + biotite + plagioclase + liquid. This triangular field provides the best *P–T* estimates of the peak metamorphic stage represented by the matrix assemblage, with *P–T* conditions of 7.1–9.2 kbar and 910–980 °C. The temperature range should be regarded as a minimum because the Ti component is not included in the calculations.

From sapphirine-bearing granulites in the margin of two gabbronorite bodies near Tuguiwula in the Jining area (Fig. 2), Jiao and Guo (2011) calculated from ternary feldspar thermometry that the granulites underwent UHT metamorphism at 900–1000 °C. Also at Tuguiwula there is a reaction rim of garnetite between a gabbronorite intrusion and UHT granulite. The garnetite contains an assemblage of garnet–Al-rich orthopyroxene–cordierite–sillimanite–spinel, in which the orthopyroxene contains up top 8% Al that corresponds to a temperature of 1020 °C (Jiao and Guo, 2011).

6.3. *P–T* evolution

In order to decipher the *P–T* evolution indicated by mineral reactions, the calculated pseudosection is simplified as Fig. 15, in which sapphirine, biotite and cordierite stability fields are emphasized. In this *P–T* pseudosection, sapphirine and cordierite paragneises do not exist because of the stability of the garnet + sillimanite tie-line (see also Fig. 13). The sapphirine becomes restricted to higher pressure, while cordierite tends to be stable at lower pressure. In particular, biotite remains stable up to 950–980 °C over a wide range of pressures.

The transition of the matrix assemblage (M_1) to the sapphirine + plagioclase symplectite (M_2) can be symbolized by the biotite breakdown reaction, which indicates a pressure-decrease in the *P–T* pseudosection (Fig. 14). The transition of the sapphirine + plagioclase symplectite (M_2) to the spinel + plagioclase ± cordierite ± corundum assemblage (M_3) is marked by the sapphirine breakdown reaction, which was a typical decompressional process as revealed in the *P–T* pseudosection (Fig. 14). Subsequently, the appearance of retrogressive biotite indicates a mainly cooling process as shown in the *P–T* pseudosection (Fig. 14). In summary, the evolution of the mineral assemblages in the reconstructed quantitative phase diagram (Fig. 14) enables definition of a *P–T* trajectory for the sapphirine granulites, in which the peak UHT (910–980 °C) metamorphism (M_1) was followed by near-isothermal decompression (M_2 and M_3) and by final decompression cooling (M_4).

It is worth mentioning here that the positions of the reaction lines for the transition from M_1 to M_2 and from M_2 to M_3 in Fig. 14 are not very accurate as the M_2 and M_3 mineral assemblages were controlled only by local equilibia between the garnet and symplectitic minerals (sapphirine, spinel and plagioclase).

Please cite this article in press as: Guo, J., et al., UHT sapphirine granulite metamorphism at 1.93–1.92 Ga caused by gabbronorite intrusions: Implications for tectonic evolution of the northern margin of the North China Craton. Precambrian Res. (2011), doi:10.1016/j.precamres.2011.07.020

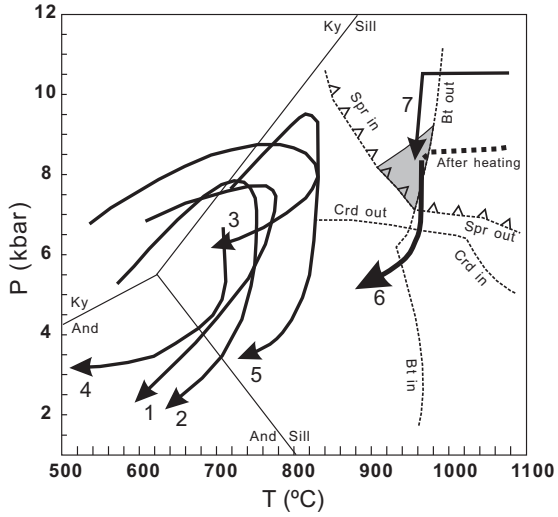

Fig. 15. *PT* diagram showing comparative metamorphic *P–T* paths of khondalite series rocks and sapphirine granulites in the Khondalite belt, North China Craton. Sapphirine, biotite and cordierite in/out lines are obtained from the *P–T* pseudosection of Fig. 14. The isothermal metamorphic *P–T* paths are: (1) Helanshan–Qianlishan Complex (Zhao et al., 1999); (2) Daqingshan–Ulashan Complex (Jin et al., 1991; Liu et al., 1993); (3) Jining Complex (first metamorphic event; Lu et al., 1992); (4) Jining Complex (second metamorphic event; Lu et al., 1992); (5) north of Datong (Liu et al., 1997). *P–T* paths of UHT granulites from the Khondalite belt: (6) isothermal path of silica-undersaturated sapphirine granulites from the Daqinshan area (taken from Fig. 14; this study); (7) isobaric curve from sapphirine granulites from the Jining area (Santosh et al., 2007a,b, 2008, 2009b). The invariant point and univariant curves in the Al_2SiO_5 system are from Holdaway (1971).

7. Discussion

7.1. Tectonic environment

The tectonic environment(s) responsible for UHT metamorphism is an interesting and topical tectono-metamorphic problem. However, in spite of numerous case studies and innovative models there is still little unanimity, because a variety of environments seem to be capable of providing the required UHT conditions. Possible settings include: 1. A back-arc basin of an active accretionary-extensional margin or orogen (Harley, 1989, 2008; Collins, 2002; Brown, 2006, 2007a,b, 2009). 2. Ridge subduction and formation of a slab window during active subduction of an ocean (Santosh and Kusky, 2010). 3. In the roots of arcs during the emplacement of magmas and subsequent granulite facies metamorphism (Jagoutz et al., 2007). 4. Post-collisional slab break-off and delamination (Harley, 2008). 5. In the deep thrust-thickened crust of a continent–continent collisional orogenic belt that underwent isothermal exhumation (Tsunogae et al., 2008). 6. As a result of magmatic underplating in a thickened crust that was undergoing extension and with an anticlockwise *PT* path (Harley, 1989; Sajeev and Osanai, 2004). 7. Post-collisional extension, intracontinental rifting and mantle plume (Santosh and Omori, 2008a,b). 8. Contact metamorphism against high-temperature intrusions such as anorthosite (McFarlane et al., 2003), charnockite (Barbosa et al., 2006), or gabbronorite (Arima and Gower, 1991). Such intrusions could be emplaced in several of the above tectonic settings. We shall now consider the most likely environment for formation of the UHT metamorphism of the Khondalite belt.

The Khondalite belt formed at c. 1.95 Ga as a result of continent–continent collision between the Yinshan block in the north and the Ordos block to the south (Zhao et al., 2005; Wu et al., 2006; Lu et al., 2008; Yin et al., 2009, 2011), and this provides a viable tectonic model to explain the *P–T* evolution of the contemporaneous Khondalite belt. Available metamorphic data show that most of the khondalitic meta-sedimentary rocks in the Khondalite belt preserve prograde, peak and post-peak mineral assemblages (M_1–M_4 of this paper; Jin et al., 1991; Lu et al., 1992; Lu and Jin, 1993; Liu et al., 1997; Zhao et al., 1999), which with their thermobarometric estimates define clockwise *P–T* paths (see Fig. 15) that mostly involve near-isothermal decompression after peak metamorphism. Such *P–T* paths, which are commonly interpreted to reflect a tectonic process of initial crustal thickening and subsequent exhumation, would be consistent with the idea that the Khondalite belt as a whole formed by continent–continent collision (Zhao et al., 2005).

However, such a continent–continent collision model that only involves crustal thickening and exhumation is not easily applicable to the specific UHT metamorphism of the sapphirine granulites from Daqingshan and Jining (e.g. Santosh et al., 2007a) for two reasons:

1 . The UHT metamorphism of the Jining sapphirine granulites is characterized by an anticlockwise *P–T* path (see trajectory No. 7 in Fig. 15), which is defined by the mineral assemblages: (1) orthopyroxene + sapphirine + sillimanite + garnet + quartz + biotite + spinel ($T > 1030\,^{\circ}C$), (2) orthopyroxene + sillimanite + quartz + garnet ($P > 10$ kbar; $T > 950\,^{\circ}C$) and (3) garnet + cordierite + orthopyroxene + quartz ($P < 10$ kbar; $T \sim 950\,^{\circ}C$) (Santosh et al., 2007a, 2008, 2009b). However, such an anticlockwise *P–T* evolution is difficult to explain by a tectonic process that involved initial crustal thickening and subsequent exhumation.
2 . The silica-undersaturated sapphirine granulites from the Daqingshan area also experienced UHT metamorphism, represented by the typical mineral assemblage garnet + sapphirine + spinel + sillimanite + biotite, although this does not contain orthopyroxene, which is common in the Jining sapphirine granulites (Santosh et al., 2007a). Moreover, the Daqingshan sapphirine granulites contain well-preserved symplectites of sapphirine + plagioclase ± rutile and spinel + plagioclase ± cordierite ± corundum that formed after the peak UHT metamorphism, and a late retrogressive assemblage of biotite + rutile + ilmenite. Using the THERMOCALC program, we constructed a pseudosection of the NCKFMASH system based on the measured bulk composition in order to estimate the *P–T* conditions and evolution of the mineral assemblages in the Daqingshan sapphirine granulites. As shown in Figs. 14 and 15, the reconstructed *P–T* path indicates that the Daqingshan sapphirine granulites underwent rapid exhumation or uplift following the peak UHT metamorphism. In addition, the result also demonstrates that the temperature of the peak UHT metamorphism of the Daqingshan sapphirine granulites was as high as 910–980 °C (Fig. 14). However, simple crustal thickening caused by continent–continent collision cannot achieve an advective geothermal gradient that would give rise to such high-temperature metamorphism (Harley, 1998a,b,c, 2004, 2008). Thus, it is unlikely that the UHT metamorphism in the Daqinghan area was directly caused by crustal thickening and rapid exhumation on an isothermal *P–T* trajectory. Another process was most likely involved.

7.2. Chronology of events

It is useful at this point to summarize the main events with their isotopic ages that contributed to the evolution of the Khondalite belt, because ideally it should be possible to relate these events and their respective igneous and metamorphic processes to the overall tectonic evolution, and we need to separate the timing and meaning of the UHT metamorphism from that of other events. We summarize isotopic data below from Zhao (2001), Zhao et al. (2005),

Please cite this article in press as: Guo, J., et al., UHT sapphirine granulite metamorphism at 1.93–1.92 Ga caused by gabbronorite intrusions: Implications for tectonic evolution of the northern margin of the North China Craton. Precambrian Res. (2011), doi:10.1016/j.precamres.2011.07.020

Xia et al. (2006a,b, 2008), Wan et al. (2006, 2009), Santosh et al. (2007a,b, 2009a), Peng et al. (2010, 2011), and references therein, and place them into a new interpretive tectonic framework:

2.1–1.96 Ga. Age of provenance rocks from which the khondalitic sediments were derived (Xia et al., 2006a,b, 2008; Wan et al., 2006; Yin et al., 2009, 2011). This is in agreement with the age of 2090 ± 22 Ma of cores of detrital zircons from the Jining area (Santosh et al., 2007b).
~2.0–1.95 Ga. Likely time of deposition of youngest sediments on a probable passive continental margin.
~1.95 Ga. Granulite facies metamorphism and deformation of the sediments that gave rise to the mineral assemblages and structural fabric of the khondalites. This includes anatexis at 1.95 Ga of impure marbles that gave rise to carbonatites (Wan et al., 2008), and the 1.95 Ga age of metamorphism in the Qianlishan and Helanshan Complexes (Yin et al., 2009, 2011). We agree with Wan et al. (2008) and Yin et al. (2009, 2011), who distinguished this 1.95 Ga metamorphic event from the 1.93 Ga to 1.92 Ga UHT metamorphic event, and with the fact that Yin et al. (2009, 2011) interpreted the former as a result of collision tectonics. We consider that the 1.95 Ga regional high-grade metamorphic and structural events can be best correlated with the collision of the Yinshan and Ordos blocks.
1.93–1.92 Ga. Main intrusion age of gabbronorite dykes/sills and plutons (Peng et al., 2010, 2011).
1.93–1.92 Ga. Time of formation of UHT metamorphism (e.g. 1917 ± 48 Ma, Santosh et al., 2007a; 1919–1923 Ma, Santosh et al., 2007b). We follow Peng et al. (2010) in demonstrating for the first time that the additional heat necessary for the UHT metamorphism was supplied by the intrusion of gabbronorites into already high-grade khondalitic rocks. A gabbronorite at Jining has a conventional U–Pb zircon age of 1921 ± 1 Ma (Guo et al., 2001), which is similar to the metamorphic age of ~1.92 Ga of the nearby sapphirine granulites (Santosh et al., 2007b).
1.93–1.89 Ga. Emplacement of S-type, garnet-bearing crustal melt granitoids that were generated from the same heat source that gave rise to the gabbronorites and the UHT metamorphism. Peng et al. (2010) described evidence of co-mingling of the gabbronorite and granitoid magmas.
1.93–1.88 Ga. Eruption of (continental) arc-type volcanics, which could be respectively cogenetic with those Xuwujia gabbronoritic intrusions and Liangcheng granitoids (Peng et al., 2011).
~1.86 Ga. Age of metamorphic rims of some zircons in the UHT sapphirine granulites, and the age of metamorphic zircons (1857 ± 4 Ma) in the Xigou recrystallized gabbro (Peng et al., 2010). This metamorphism is not pervasive throughout the Khondalite belt, but it was responsible for partial recrystallization of the gabbronorites, and associated deformation caused foliation and folding of the smallest gabbronorite dykes/sills. This ~1.86 Ga metamorphic age is coincident with the well-defined 1.85 Ga age of formation of the Trans-North China Orogen (Zhao, 2001; Zhao et al., 2002a, 2008a,b; Wilde et al., 2002, 2004a,b; Guo et al., 2005; Kröner et al., 2005, 2006; Wilde and Zhao, 2005; Liu et al., 2006), and with the 2.0–1.8 Ga time of assembly of the Columbia supercontinent (Zhao et al., 2002b, 2003b, 2004; Wan et al., 2009).

7.3. Correlations with orogenic events

A major problem with some earlier papers on the Khondalite belt was that there was no means of distinguishing earlier from later metamorphic and isotopic events, and this led to confusing conclusions with regard to correlations with tectonic/orogenic events. For example, Santosh et al. (2007b) interpreted the age of ~1920 Ma, obtained from UHT rocks in the Jining area, as 'the time of peak granulite facies metamorphism in the Khondalite belt that was directly related to the collision between the Yinshan and Ordos blocks', and therefore concluded that this 'UHT metamorphic age correlates well with the time of assembly of the Paleoproterozoic Columbia supercontinent'.

In order to constrain the available isotopic data in relation to interpret tectonic events, and to help resolve arguments and interpretations about correlations with the time of formation of orogenic belts and the consequent history or closure times of oceans, we present the following rationale.

The discovery of consistent contiguous relationships between 1.95 Ga and 1.92 Ga gabbronorite intrusions and 1.93–1.92 Ga UHT metamorphic rocks in the Khondalite belt enabled Peng et al. (2010) to demonstrate that the additional heat required for the UHT metamorphism was provided by the high-temperature intrusions. The peak metamorphic temperature of the Khondalite belt was 700–820 °C (Jin et al., 1991; Lu et al., 1992; Lu and Jin, 1993; Liu et al., 1997), and the UHT metamorphism in general took place at 900–1000 °C (Jiao and Guo, 2011); thus an increase of temperature of about 100–200 °C was responsible for the local increase above the regional peak metamorphic temperature.

Here we use the gabbronorite dykes and sills to distinguish earlier from later orogenic events, following the long-established principle that deformed and metamorphosed basic dykes enable separation of two orogens (e.g. Sutton and Watson, 1951 who separated the Scourian and Laxfordian events within the Lewisian complex of NW Scotland).

Working backwards in time, the 1.95–1.92 Ga gabbronorite dykes and sills are locally deformed and metamorphosed, and the youngest zircons in the sapphirine granulites and the Xigou intrusion in the Khondalite belt have zircon ages of ~1.86 Ga. We suggest that this last orogenic event can be best correlated with the coeval 1.85 Ga collision between the Western and Eastern blocks of the North China Craton that created the Trans-North China Orogen. It is reasonable to infer that the formation of this huge collisional orogenic belt had a metamorphic–structural influence on the overriding upper plate in which the Khondalite belt was situated.

This scenario also implies that westwards subduction of the earlier Trans-North China ocean under an active continental margin represented by the unified Yinshan–Ordos block likely had an influence on the generation of the gabbronorite magmatism in the period 1.95–1.92 Ga, Peng et al. (2010, 2011) made the suggestion, with which we agree, that the gabbronorite magmatism was likely created by a process of ridge subduction, which would have provided the high temperatures required for generation of the gabbronorite magma, as well as for the consequent formation of the UHT metamorphism at 1.93–1.92 Ga, and for the partial melting of deep crust to create the 1.93–1.89 Ga S-type garnet-rich granitoids. From the high-Mg composition of some key gabbronorites, Peng et al. (2010) calculated that the mantle potential temperature was ~1550 °C, which is higher than the ~1500 °C temperature of the Palaeoproterozoic ambient mantle, and that the primary eruption temperature was ~1400 °C, which is appropriate for formation of the extreme UHT metamorphism. Ridge subduction as a result of ridge–trench interaction is well known as a model mechanism to explain the generation of magmas and HT and UHT metamorphism (DeLong et al., 1979; Iwamori, 2000; Sisson et al., 2003; Santosh and Kusky, 2010). Thus, we conclude that in the Khondalite belt, ridge subduction was responsible for mantle melting that largely gave rise to the gabbronorite intrusions, for deep crustal melting that gave to the contemporaneous garnet granites, and for the UHT metamorphism, which developed against and soon after the intrusive gabbronorite intrusions.

The gabbronorite dykes, sills and plutons commonly transect discordantly the foliation of the 1.95 Ga granulite facies khondalites. Accordingly, we consider that the Khondalite belt was most likely created at ~1.95 Ga during formation of the orogenic belt that

Please cite this article in press as: Guo, J., et al., UHT sapphirine granulite metamorphism at 1.93–1.92 Ga caused by gabbronorite intrusions: Implications for tectonic evolution of the northern margin of the North China Craton. Precambrian Res. (2011), doi:10.1016/j.precamres.2011.07.020

resulted from collision between the Yinshan and Ordos blocks. This is consistent with available geological and isotopic data (Zhao et al., 2005; Yin et al., 2009, 2011).

Finally, we note that the Khondalite belt in China is not alone in containing gabbronorite or other HT intrusions that are bordered by UHT 'contact' metamorphism. For example, a gabbronorite intrusion in the Grenville orogen in Labrador was responsible for formation of sapphirine-bearing UHT assemblages at a temperature of ~1000 °C (Arima and Gower, 1991), and temperatures up to 900 °C were developed in gneisses against an olivine–orthopyroxene granite cored by troctolite and anorthosite in the Nain Plutonic Suite in Labrador (McFarlane et al., 2003). In Algeria a 2002 Ma anorthosite–carbonatite intrusion created a coeval contact zone of sapphirine-bearing, silica-undersaturated granulite facies assemblages at 800–1100 °C (Ouzegane et al., 2003), in SW Norway UHT assemblages increase towards the Rogaland anorthosite complex (Westphal et al., 2003), and in Brazil UHT granulites were produced against a charnockite pluton at a temperature of 900–1000 °C only 50 °C above the ambient regional metamorphic temperature (Barbosa et al., 2006). All these well-documented examples demonstrate that given the right bulk compositions it is possible to generate local UHT conditions in HT granulites close to HT intrusions. These conclusions about the role of a magmatic heat source in the production of UHT metamorphism are supported and constrained by quantitative thermal modeling of high-temperature isograde, conductive heat flow, and thermal gradients against intrusions of different sizes by McFarlane et al. (2003) and Westphal et al. (2003).

Acknowledgements

We thank L.Q. Zhang, T.S. Li, F. Liu, L. Chen, Z.W. Lan, and X.D. Ma for their assistance in the field work, and Q. Mao and Y.G. Ma for their technical support with the microprobe analyses. J. Wheeler and S.G. Song are thanked for constructive reviews. We also thank S. Harley, E. Grew and M. Santosh for their helpful comments on the early version of this manuscript. Most of all, J.H. Guo is very grateful to G.C. Zhao for thorough and constructive discussions and valuable assistance on this paper. This work was financed by Chinese NSFC grants (Nos. 40730315 and 40372089).

Appendix A. Supplementary data

Supplementary data associated with this article can be found, in the online version, at doi:10.1016/j.precamres.2011.07.020.

References

Arima, M., Gower, C.F., 1991. Osumilite-bearing granulites in the Eastern Grenville Province, Eastern Labrador, Canada: mineral paragneises and metamorphic conditions. J. Petrol. 32, 29–61.
Barbosa, J., Nicollet, C., Leite, C., Kienast, J.R., Fuck, R.A., Macedo, E.P., 2006. Hercynite-quartz-bearing granulites from Brejões Dome area, Jequié block, Bahia, Brazil: influence of charnockite intrusion on granulite-facies metamorphism. Lithos 92, 537–556.
Brown, M., 2006. Duality of thermal regimes is the distinctive characteristic of plate tectonics since the Neoarchaean. Geology 34, 961–964.
Brown, M., 2007a. Metamorphic conditions in orogenic belts: a record of secular change. Int. Geol. Rev. 49, 193–234.
Brown, M., 2007b. Metamorphism, plate tectonics, and the supercontinent cycle. Earth Sci. Front. 14, 1–18.
Brown, M., 2009. Metamorphic patterns in orogenic systems and the geological record. In: Cawood, P.A., Kröner, A. (Eds.), Earth Accretionary systems in Space and Time. Special Publications 318. Geological Society, London, pp. 37–74.
Cesare, B., Satish-Kumar, M., Cruciani, G., Pocker, S., Nodari, L., 2008. Mineral chemistry of Ti-rich biotite from pegmatite and metapelitic granulites of the Kerala Khondalite Belt (southeast India): petrology and further insight into titanium substitutions. Am. Mineral. 93, 327–338.
Collins, W.J., 2002. Hot orogens, tectonic switching and creation of continental crust. Geology 31, 535–538.
Condie, K.C., Boryta, M.D., Liu, J.Z., 1992. The origin of khondalites: geochemical evidence from the Archean to Early Proterozoic granulite belt in the North China craton. Precambrian Res. 59, 207–223.
DeLong, S.E., Schwarz, W.M., Anderson, R.N., 1979. Thermal effects of ridge subduction. Earth Planet. Sci. Lett. 44, 239–246.
Faure, M., Trap, P., Lin, W., Monie, P., Bruguier, O., 2007. Polyorogenic evolution of the Paleoproterozoic Trans-North China Belt, new insights from the Lüliangshan-Hengshan-Wutaishan and Fuping massifs. Episodes 30, 1–12.
Fuhrman, M.L., Lindsley, D.H., 1988. Ternary-feldspar modeling and thermometry. Am. Mineral. 73, 201–215.
Guo, J.H., Zhai, M.G., Xu, R.H., 2001. Timing of the granulite facies metamorphism in the Sanggan area, North China craton: zircon U–Pb geochronology. Sci. China Ser. D44, 1010–1018.
Guo, J.H., Chen, Y., Peng, P., Liu, F., Chen, L., Zhang, L.Q., 2006. Sapphirine granulite from Daqingshan area, Inner Mongolia – 1. 85 Ga ultrahigh temperature (UHT) metamorphism. In: Proceedings of National Conference on Petrology and Geodynamics in China (Nanjing), pp. 215–218.
Guo, J.H., O'Brien, P.J., Zhai, M.G., 2002. High-pressure granulites in the Sangan area, North China Craton: metamorphic evolution, P–T paths and geotectonic significance. J. Metamorph. Geol. 20, 741–756.
Guo, J.H., Sun, M., Zhai, M.G., 2005. Sm–Nd and SHRIMP U–Pb zircon geochronology of high-pressure granulites in the Sanggan area, North China Craton: timing of Paleoproterozoic continental collision. J. Asian Earth Sci. 24, 629–642.
Guo, J.H., Shi, X., Bian, A.G., Xu, R.H., Zhai, M.G., Li, Y.G., 1999. Pb isotopic composition of feldspar and U-Pb age of zircon from early Proterozoic granite in Sanggan area, North China craton: metamorphism, crustal melting and tectono-thermal event. Acta Petrologica Sinica 15 (2), 199–207 (in Chinese with English abstract).
Harley, S.L., 1989. The origins of granulites: a metamorphic perspective. Geol. Mag. 126, 215–247.
Harley, S.L., 1992. Proterozoic granulite terranes. In: Condie, K.C. (Ed.), Proterozoic Crustal Evolution. Elsevier, Amsterdam, pp. 301–360.
Harley, S.L., 1998a. On the occurrence and characterisation of ultrahigh-temperature (UHT) crustal metamorphism. In: Treloar, P.J., O'Brien, P. (Eds.), What Controls Metamorphism and Metamorphic Reactions? Special Publication, vol. 138. Geological Society of London, pp. 75–101.
Harley, S.L., 1998b. An appraisal of peak temperatures and thermal histories in ultrahigh-temperature (UHT) crustal metamorphism: the significance of aluminous orthopyroxene. In: Motoyoshi, Y., Shiraishi, K. (Eds.), Origin and Evolution of Continents. Memoir National Institute Polar Research, Tokyo, pp. 49–73 (special Issue 53).
Harley, S.L., 1998c. Ultrahigh temperature granulite metamorphism (1050 °C, 12 kbar) metamorphism and decompression in garnet (Mg70)- orthopyroxene-sillimanite gneisses from the Rauer Group, East Antarctica. J. Metamorph. Geol. 16, 541–562.
Harley, S.L., 2004. Extending our understanding of ultrahigh temperature crustal metamorphism. J. Mineral. Petrol. Sci. 99, 140–158.
Harley, S.L., 2008. Refining the *P-T* records of UHT crustal metamorphism. J. Metamorph. Geol. 26, 125–154.
Hayob, J.L., Essene, E.J., Ruiz, J., Ortega-Gutierrez, F., Aranda-Gomez, J.J., 1989. Young high-temperature granulites from the base of the crust in central Mexico. Nature 342, 265–268.
Henry, D.J., Guidotti, C.V., Thomson, J.A., 2005. The Ti-saturation surface for low-to-medium pressure metapelitic biotite: implications for geothermometry and Ti-substitution mechanisms. Am. Mineral. 90, 316–328.
Hokada, T., 2001. Feldspar geothermometer in ultrahigh temperature metamorphic rocks: evidence of crustal metamorphism attaining ~1100 °C in the Archaean Napier Complex, East Antarctica. Am. Mineral. 86, 932–938.
Hokada, T., Suzuki, S., 2006. Feldspar in felsic orthogneiss as indicator for UHT crustal processes. J. Mineral. Petrol. Sci. 101, 260–264.
Holdaway, M.J., 1971. Stability of andalusite and the aluminium silicate phase diagram. Am. J. Sci. 271, 97–131.
Holland, T.J.B., Powell, R., 1998. An internally consistent thermodynamic data set for phases of petrological interest. J. Metamorph. Geol. 16, 309–343.
Iwamori, H., 2000. Thermal effects of ridge subduction and its implications for the origin of granitic batholiths and paired metamorphic belts. Earth Planet. Sci. Lett. 181, 131–144.
Jagoutz, O., Müntener, o., Ulmer, P., Pettke, T., Burg, J.-P., Dawood, H., Hussain, S., 2007. Petrology and mineral chemistry of lower crustal intrusions: the Chilas Complex, Kohistan (NW Pakistan). J. Petrol. 48, 1896–1953.
Jiao, S.H., Guo, J.H., 2011. Application of the two-feldspar geothermometer to ultrahigh-temperature (UHT) rocks in the Khondalite belt, North China craton and its implications. Am. Mineral. 96, 250–260.
Jin, W., 1989. Early Precambrian geological evolution and metamorphic study on the basement of the north margin of the North China platform. Unpublished PhD thesis, Changchun College of Geology, China (in Chinese).
Jin, W., Li, S.X., Liu, X.S., 1991. The metamorphic dynamics of Early Precambrian high-grade metamorphic rocks series in Daqing-Ulashan area, Inner Mongolia. Acta Petrologica Sinica 4, 27–35 (in Chinese with English abstract).
Kelsey, D.E., 2008. On the ultrahigh-temperature crustal metamorphism. Gondwana Res. 13, 1–29.
Kelsey, D.E., White, R.W., Holland, T.J.B., Powell, R., 2004. Calculated phase equilibria in K_2O–MgO–FeO–Al_2O_3–SiO_2–H_2O for sapphirine–quartz-bearing mineral assemblages. J. Metamorph. Geol. 22, 559–578.
Kelsey, D.E., White, R.W., Powell, R., 2005. Calculated phase equilibria in K_2O-FeO-MgO -Al_2O_3-SiO_2-H_2O for silica-undersaturated sapphirine-bearing mineral assemblages. J. Metamorph. Geol. 23, 217–239.

Kretz, R., 1983. Symbols for rock-forming minerals. Am. Mineral. 68, 277–279.
Kröner, A., Wilde, S.A., Li, J.H., Wang, K.Y., 2005. Age and evolution of a late Archaean to early Paleozoic upper to lower crustal section in the Wutaishan/Hengshan/Fuping terrain of northern China. J. Asian Earth Sci. 24, 577–595.
Kröner, A., Wilde, S.A., Zhao, G.C., O'Brien, P.J., Sun, M., Liu, D.Y., Wan, Y.S., Liu, S.W., Guo, J.H., 2006. Zircon geochronology of mafic dykes in the Hengshan Complex of northern China: evidence for late Palaeoproterozoic rifting and subsequent high-pressure event in the North China Craton. Precambrian Res. 146, 45–67.
Kusky, T.M., Li, J.H., 2003. Paleoproterozoic tectonic evolution of the North China Craton. J. Asian Earth Sci. 22, 383–397.
Kusky, T.M., Li, J.H., Santosh, M., 2007. The Paleoproterozoic North Hebei Orogen: North China craton's collisional suture with the Columbia supercontinent. Gondwana Res. 12, 4–28.
Li, J.H., Kusky, T.M., 2007. A late Archean foreland fold and thrust belt in the North China Craton: implications for early collisional tectonics. Gondwana Res. 12, 47–66.
Li, J.H., Qian, X.L., Liu, S.W., 2000. Geochemistry of khondalites from central portion of North China craton (NCC): implications for the continental cratonization in the Neoarchean. Sci. China Ser. D43, 253–265.
Li, S.Z., Zhao, G.C., Zhang, J., Sun, M., Zhang, G.W., Luo, D., 2010. Deformational history of the Hengshan-Wutai-Fuping belt: implications for the evolution of the Trans-North China Orogen. Gondwana Res. 18, 611–631.
Liu, C.H., Zhao, G.C., Sun, M., Wu, F.Y., Yang, J.H., Yin, C.Q., Leung, W.H., 2011. U-Pb and Hf isotopic study of detrital zircons from the Yejishan Group of the Lüliang Complex: constraints on the timing of collision between the Eastern and Western Blocks, North China Craton. Sedimentary Geol. 236, 129–140.
Liu, F.L., Shen, Q.H., Geng, Y.S., Xu, X.C., Ma, R., 1997. Experimental study of melting reaction and genetic mechanism of mineral phase transformation in granulite facies metamorphism. Acta Geologoca Sinica 71, 254–265 (in Chinese with English Abstract).
Liu, J.Z., Qiang, X.K., Liu, X.S., Ouyang, Z.Y., 2000. Dynamics and genetic grids of sapphirine-bearing spinel gneiss in Daqing Mountain orogen zone, Inner Mongolia. Acta Petrologica Sinica 16, 245–255 (in Chinese with English abstract).
Liu, S.W., Zhao, G.C., Wilde, S.A., Shu, G.M., Sun, M., Li, Q.G., Tian, W., Zhang, J., 2006. Th-U–Pb monazite geochronology of the Lüliang and Wutai Complexes: constraints on the tectonothermal evolution of the Trans-North China Orogen. Precambrian Res. 148, 205–225.
Liu, S.J., Li, J.H., Santosh, M., 2010. First application of the revised Ti-in-zircon geothermometer to Paleoproterozoic ultrahigh-temperature granulites of Tuguiwula, Inner Mongolia, North China Craton. Contrib. Mineral. Petr. 159, 225–235.
Liu, X.S., Jin, W., Li, S.X., Xu, X.C., 1993. Two types of Precambrian high-grade metamorphism, Inner Mongolia, China. J. Metamorph. Geol. 11, 499–510.
Lu, L.Z., Jin, S.Q., 1993. *P-T*-t paths and tectonic history of an early Precambrian granulite facies terrane, Jining district, southeastern Inner Mongolia, China. J. Metamorph. Geol. 11, 483–498.
Lu, L.Z., Jin, S.Q., Xu, X.T., Liu, F.L., 1992. Petrogenesis and Mineralization of Khondalite Series in Southeastern Inner Mongolia. Jilin Science and Technology Press, Changchun, China, 156 p. (in Chinese with English abstract).
Lu, L.Z., Xu, X.C., Liu, F.L., 1996. Early Precambrian Khondalite Series in North China. Changchun Publishing House, Changchun, China, 276 p. (in Chinese with English abstract).
Lu, S.N., Zhao, G.C., Wang, H.C., Hao, G.J., 2008. Precambrian metamorphic basement and sedimentary cover of the North China Craton: review. Precambrian Res. 160, 77–93.
McFarlane, C.R.M., Carlson, W.D., Connelly, J.N., 2003. Prograde, peak, and retrograde *P-T* paths from aluminium in orthopyroxene: high-temperature contact metamorphism in the aureole of the Makhavinekh Lake pluton, Nain Plutonic Suite, Labrador. J. Metamorph. Geol. 21, 405–423.
Ouzegane, K., Guiraud, M., Kienast, J.R., 2003. Prograde and retrograde evolution in high-temperature corundum granulites (FMAS and KFMASH systems) from In Ouzzal terrane, NW Hoggar, Algeria. J. Petrol. 44, 517–545.
Patiño Douce, A.E., 1993. Titanium substitution in biotite: an empirical model with applications to thermometry, O_2 and H_2O barometries, and consequences for biotite stability. Chem. Geol. 108, 133–162.
Peng, P., Guo, J.-H., Zhai, M.-G., Bleeker, W., 2010. Paleoproterozoic gabbronoritic and granitic magmatism in the northern margin of the North China Craton: evidence of crust–mantle interaction. Precambrian Res. 183, 635–659.
Peng, P., Guo, J., Windley, B.F., Li, X., 2011. Halaqin volcano-sedimentary succession in the central-northern margin of the North China Craton: products of Late Paleoproterozoic ridge subduction. Precambrian Res., doi:10.1016/j.precamres.2011.03.006.
Peng, P., Zhai, M.-G., Zhang, H.F., Guo, J.H., 2005. Geochronological constraints on the Paleoproterozoic evolution of the North China Craton: SHRIMP zircon ages of different types of mafic dikes. Int. Geol. Rev. 47, 492–508.
Pilugin, S.M., Fonarev, V.I., Savko, K.A., 2009. Feldspar geothermometer of ultrahigh-temperature (≥1000 °C) metapelites from the Voronezh crystalline massif, Kursk–Besedino Granulite Block. Doklady Earth Sci. 425, 201–204.
Powell, R., Holland, T.J.B., Worley, B., 1998. Calculating phase diagrams involving solid solutions via non-linear equations, with examples using THERMOCALC. J. Metamorph. Geol. 6, 173–204.
Prakash, D., Arima, M., Mohan, A., 2006. Ultrahigh-temperature metamorphism in the Palni Hills, South India: insights from feldspar thermometry and phase equilibria. Int. Geol. Rev. 48, 619–638.
Qian, X.L., Li, J.H., 1999. The discovery of Neoarchean unconformity and its implication for continental cratonization of North China Craton. Sci. China Ser. D 42, 401–407.
Sajeev, K., Osanai, Y., 2004. Ultrahigh-temperature metamorphism (1150 °C, 12 kbar) and multistage evolution of Mg-Al-rich granulites from the Central Highland Complex, Sri Lanka. J. Petrol. 45, 1821–1844.
Santosh, M., Omori, S., 2008a. CO_2 windows from mantle to atmosphere: models on ultrahigh-temperature metamorphism and speculations on the link with melting of snowball Earth. Gondwana Res. 14, 82–96.
Santosh, M., Omori, S., 2008b. CO_2 flushing: a plate tectonic perspective. Gondwana Res. 13, 86–102.
Santosh, M., Kusky, T., 2010. Origin of paired high pressure–ultrahigh-temperature orogens: a ridge subduction and slab window model. Terra Nova 22, 35–42.
Santosh, M., Sajeev, K., Li, J.H., 2006. Extreme crustal metamorphism during Columbia supercontinent assembly: evidence from North China Craton. Gondwana Res. 10, 256–266.
Santosh, M., Sajeev, K., Li, J.H., Liu, S.J., Itaya, T., 2009b. Counterclockwise exhumation of a hot orogen: the Paleoproterozoic ultrahigh-temperature granulites in the North China Craton. Lithos 110, 140–152.
Santosh, M., Tsunogae, T., Li, J.H., Liu, S.J., 2007a. Discovery of sapphirine-bearing Mg-Al granulites in the North China Craton: implications for Paleoproterozoic ultrahigh temperature metamorphism. Gondwana Res. 11, 263–285.
Santosh, M., Tsunogae, T., Ohyama, H., Sato, K., Li, J.H., Liu, S.J., 2008. Carbonic metamorphism at ultrahigh-temperatures: evidence from North China Craton. Earth Planet. Sci. Lett. 266, 149–165.
Santosh, M., Wan, Y., Liu, D., Dong, C., Li, J., 2009a. Anatomy of zircons from an ultrahot orogen: the amalgamation of North China Craton within the supercontinent Columbia. J. Geol. 117, 429–443.
Santosh, M., Wilde, S.A., Li, J.H., 2007b. Timing of Paleoproterozoic ultrahigh-temperature metamorphism in the North China Craton: evidence from SHRIMP U–Pb zircon geochronology. Precambrian Res. 159, 178–196.
Santosh, M., Zhao, D., Kusky, T., 2010. Mantle dynamics of the Paleoproterozoic North China Craton: a perspective based on seismic tomography. J. Geodyn. 49, 39–53.
Sisson, V.B., Pavlis, T.L., Roeske, S.M., Thorkelson, D.J., 2003. Introduction: an overview of ridge-trench interactions in modern and ancient settings. In: Sisson, V.B., Roeske, S.M., Pavlis, T.L. (Eds.), Geology of a Transpressional Orogen during Ridge-Trench Interaction along the North Pacific Margin. Geological Society of America Special Paper 371, pp. 1–18.
Sutton, J., Watson, J.V., 1951. The pre-Torridonian metamorphic history of the Loch Torridon and Scourie areas of the north-west Highlands and its bearing on the chronological classification of the Lewisian. J. Geol. Soc. Lond. 106, 241–296.
Trap, P., Faure, M., Lin, W., Monié, P., 2007. Late Paleoproterozoic (1900–1800 Ma) nappe stacking and polyphase deformation in the Hengshan-Wutaishan area: implications for the understanding of the Trans-North-China Belt, North China Craton. Precambrian Res. 156, 85–106.
Tsunogae, T., Santosh, M., Ohyama, H., Sato, K., 2008. High-pressure and ultrahigh-temperature metamorphism at Komateri, northern Madurai Block, southern India. J. Asian Earth Sci. 33, 395–413.
Wan, Y.S., Song, B., Liu, D.Y., Wilde, S.A., Wu, J.S., Shi, Y.R., Yin, X.Y., Zhou, H.Y., 2006. SHRIMP U–Pb zircon geochronology of Palaeoproterozoic metasedimentary rocks in the North China Craton: evidence for a major Late Palaeoproterozoic tectonothermal event. Precambrian Res. 149, 249–271.
Wan, Y.S., Liu, D.Y., Dong, C.Y., Xu, Z.Y., Wang, Z.J., Wilde, S.A., Yang, Y.H., Liu, Z.H., Zhou, H.Y., 2009. The Precambrian khondalite belt in the Daqingshan area, North China craton: evidence for multiple metamorphic events in the Palaeoproterozoic era. In: Reddy, S.M., Mazumder, R., Evans, D.A.D., Collins, A.S. (Eds.), Palaeoproterozoic Supercontinents and Global Evolution. Special Publications 323. Geological Society, London, pp. 73–97.
Wan, Y.S., Liu, D.Y., Xu, Z.Y., Dong, C.Y., Wang, Z.J., Zhou, H.Y., Yang, Z.S., Liu, Z.H., Wu, J.S., 2008. Paleoproterozoic crustally derived carbonate-rich magmatic rocks from the Daqingshan area, North China craton: geological, petrographical, geochronological and geochemical (Hf, Nd, O and C) evidence. Am. J. Sci. 308, 351–378.
Wang, Z.H., 2009. Tectonic evolution of the Hengshan-Wutai-Fuping complexes and its implication for the Trans-North China Orogen. Precambrian Res. 170, 73–87.
Wang, Z.H., 2010. Reply to the comment by Zhao et al. on: "Tectonic evolution of the Hengshan-Wutai-Fuping complexes and its implication for the Trans-North China Orogen" [Precambrian Res., 170 (2009) 73-87]. Precambrian Res. 176, 99–104.
Wang, J., Wu, Y.B., Gao, S., Peng, M., Liu, X.C., Zhao, L.S., Zhou, L., Hu, Z.C., Gong, H.J., Liu, Y.S., 2010a. Zircon U-Pb and trace element data from rocks of the Huai'an Complex: new insights into the late Paleoproterozoic collision between the Eastern and Western Blocks of the North China Craton. Precambrian Res. 178, 59–71.
Wang, Z.H., Wilde, S.A., Wan, J.L., 2010b. Tectonic setting and significance of 2.3-2.1 Ga magmatic events in the Trans-North China Orogen: new constraints from the Yanmenguan mafic-ultramafic intrusion in the Hengshan-Wutai-Fuping area. Precambrian Res. 178, 27–42.
Wang, F., Li, X.P., Chu, H., Zhao, G.C., 2011. Petrology and metamorphism of khondalites from Jining Complex in the North China Craton. Int. Geol. Rev. 53, 212–229.
Westphal, M., Schumacher, J.C., Boschert, S., 2003. High-temperature metamorphism and the role of magmatic heat sources at the Rogaland anorthosite complex in southwestern Norway. J. Petrol. 44, 1145–1162.
Wilde, S.A., Zhao, G.C., Sun, M., 2002. Development of the North China Craton during the Late Archaean and its final amalgamation at 1.8 Ga; some speculations on

Please cite this article in press as: Guo, J., et al., UHT sapphirine granulite metamorphism at 1.93–1.92 Ga caused by gabbronorite intrusions: Implications for tectonic evolution of the northern margin of the North China Craton. Precambrian Res. (2011), doi:10.1016/j.precamres.2011.07.020

its position within a global Palaeoproterozoic supercontinent. Gondwana Res. 5, 85–94.
Wilde, S.A., Zhao, G.C., 2005. Archean to Paleoproterozoic evolution of the North China Craton. J. Asian Earth Sci. 24, 519–522.
Wilde, S.A., Zhao, G.C., Wang, K.Y., Sun, M., 2004a. First precise SHRIMP U–Pb zircon ages for the HutuoGroup, Wutaishan: further evidence for the Palaeoproterozoic amalgamation of the North China Craton. Chin. Sci. Bull. 49, 83–90.
Wilde, S.A., Cawood, P.A., Wang, K.Y., Nemchin, A., Zhao, G.C., 2004b. Determining Precambrian crustal evolution in China: a case-study from Wutaishan, Shanxi Province, demonstrating the application of precise SHRIMP U-Pb geochronology. In: Malpas, J., Fletcher, C.J.N., Ali, J.R., Aitchison, J.C. (Eds.), Aspects of the Tectonic Evolution of China, Special Publication Geological Society of London 226. , pp. 5–25.
Wu, C.H., Sun, M., Li, H.M., Zhao, G.C., Xia, X.P., 2006. LA-ICP-MS U-Pb zircon ages of the khondalites from the Wulashan and Jining high-grade terrain in northern margin of the North China Craton: constraints on sedimentary age of the khondalite. Acta Petrologica Sinica 22 (11), 2639–2654.
Xia, X.P., Sun, M., Zhao, G.C., Luo, Y., 2006a. LA-ICP-MS U–Pb geochronology of detrital zircons from the Jining Complex, North China Craton and its tectonic significance. Precambrian Res. 144, 199–212.
Xia, X.P., Sun, M., Zhao, G.C., Wu, F.Y., Xu, P., Zhang, J.H., Luo, Y., 2006b. U–Pb and Hf isotopic study of detrital zircons from the Wulashan khondalites: Constraints on the evolution of the Ordos Terrane, Western Block of the North China Craton. Earth Planet. Sci. Lett. 241, 581–593.
Xia, X.P., Sun, M., Zhao, G.C., Wu, F.Y., Xu, P., Zhang, J., He, Y.H., 2008. Paleoproterozoic crustal growth in the Western Block of the North China Craton: evidence from detrital zircon Hf and whole rock Sr-Nd isotopic compositions of the Khondalites from the Jining Complex. Am. J. Sci. 308, 304–327.
Xia, X.P., Sun, M., Zhao, G.C., Wu, F.Y., Xu, P., Zhang, J.S., 2009. Detrital zircon U-Pb age and Hf isotope study of the khondalite in Trans-North China Orogen and its tectonic significance. Geol. Mag. 146, 701–716.
Yin, C.Q., Zhao, G.H., Sun, M., Xia, X.P., Wei, C.J., Zhou, X.W., Leung, W.H., 2009. LA-ICP-MS U–Pb zircon ages of the Qianlishan Complex: constrains on the evolution of the Khondalite Belt in the Western Block of the North China Craton. Precambrian Res. 174, 78–94.
Yin, C.Q., Zhao, G.C., Guo, J.H., Sun, M., Zhou, X.W., Zhang, J., Xia, X.P., Liu, C.H., 2011. U-Pb and Hf isotopic study of zircons of the Helanshan Complex: constrains on the evolution of the Khondalite Belt in the Western Block of the North China Craton. Lithos 122, 25–38.
Zhai, M.G., Guo, J.H., Li, J.H., Li, Y.G., Yan, Y.H., Zhang, W.H., 1996. Retrograded eclogites in the Archaean North China craton and their geological implication. Chin. Sci. Bull. 41, 315–326.
Zhai, M.G., Guo, J.H., Yan, Y.H., Li, Y.G., Han, X.L., 1993. Discovery of high-pressure basic granulite terrain in North China craton and preliminary study. Sci. China (B) 36, 1402–1408.
Zhang, J., Zhao, G.C., Sun, M., Wilde, S.A., Li, S.Z., Liu, S.W., 2006. High-pressure mafic granulites in the Trans-North China Orogen: tectonic significance and age. Gondwana Res. 9, 349–362.
Zhang, J., Zhao, G.C., Li, S.Z., Sun, M., Liu, S.W., Wilde, S.A., Kröner, A., Yin, C.Q., 2007. Deformation history of the Hengshan Complex: implications for the tectonic evolution of the Trans-North China Orogen. J. Struct. Geol. 29, 933–949.
Zhang, J., Zhao, G.C., Li, S.Z., Sun, M., Wilde, S.A., Liu, S.W., Yin, C.Q., 2009. Polyphase deformation of the Fuping Complex, Trans-North China Orogen: structures, SHRIMP U–Pb zircon ages and tectonic implications. J. Struct. Geol. 31, 177–193.
Zhao, G.C., 2001. Paleoproterozoic assembly of the North China Craton. Geol. Mag. 138, 87–91.
Zhao, G.C., 2009. Metamorphic evolution of major tectonic units in the basement of the North China Craton: key issues and discussion. Acta Petrologica Sinica 25, 1772–1792.
Zhao, G.C., Wilde, S.A., Cawood, P.A., Sun, M., 2001a. Archean blocks and their boundaries in the North China Craton: lithological, geochemical, structural and *P-T* path constraints and tectonic evolution. Precambrian Res. 107, 45–73.
Zhao, G.C., Cawood, P.A., Wilde, S.A., 2001b. High-pressure granulite (retrograded eclogites) from the Hengshan Complex, North China Craton: petrology and tectonic implications. J. Petrol. 42, 1141–1170.
Zhao, G.C., Wilde, S.A., Cawood, P.A., Sun, M., 2002a. SHRIMP U-Pb zircon ages of the Fuping Complex: implications for accretion and assembly of the North China Craton. Am. J. Sci. 302, 191–226.
Zhao, G.C., Cawood, P.A., Wilde, S.A., Sun, M., 2002b. A review of the global 2.1-1.8 Ga orogens: implications for a pre-Rodinian supercontinent. Earth Sci. Rev. 59, 125–162.
Zhao, G.C., Sun, M., Wilde, S.A., Li, S.Z., 2004. A Paleo-Mesoproterozoic supercontinent: assembly, growth and breakup. Earth Sci. Rev. 67, 91–123.
Zhao, G.C., Sun, M., Wilde, S.A., 2003a. Major tectonic units of the North China Craton and their Paleoproterozoic assembly. Sci. China Ser. D 46, 23–38.
Zhao, G.C., Sun, M., Wilde, S.A., Li, S.Z., 2003b. Assembly, accretion and breakup of the Paleo-Mesoproterozoic Columbia supercontinent: records in the North China Craton. Gondwana Res. 6, 417–434.
Zhao, G.C., Sun, M., Wilde, S.A., Li, S.Z., 2005. Late Archean to Paleoproterozoic evolution of the North China Craton: key issues revisited. Precambrian Res. 136, 177–202.
Zhao, G.C., Wilde, S.A., Cawood, P.A., Lu, L.Z., 1998. Thermal evolution of the Archaean basement rocks from the eastern part of the North China Craton and its bearing on tectonic setting. Int. Geol. Rev. 40, 706–721.
Zhao, G.C., Wilde, S.A., Cawood, P.A., Lu, L.Z., 1999. Tectonothermal history of the basement rocks in the western zone of the North China Craton and its tectonic implications. Tectonophysics 310, 37–53.
Zhao, G.C., Wilde, S.A., Cawood, P.A., Lu, L.Z., 2000. Petrology and P–T path of the Fuping mafic granulites: implications for tectonic evolution of the central zone of the North China Craton. J. Metamorph. Geol. 18, 375–391.
Zhao, G.C., Wilde, S.A., Sun, M., Guo, J.H., Kroner, A., Li, S.Z., Li, X.P., Wu, C.M., 2008a. SHRIMP U–Pb zircon geochronology of the Huai'an Complex: constraints on Late Archean to Paleoproterozoic crustal accretion and collision of the Trans-North China Orogen. Am. J. Sci. 308, 270–303.
Zhao, G.C., Wilde, S.A., Sun, M., Li, S.Z., Li, X.P., Zhang, J., 2008b. SHRIMP U-Pb zircon ages of granitoid rocks in the Lüliang Complex: implications for the accretion and evolution of the Trans-North China Orogen. Precambrian Res. 160, 213–226.
Zhao, G.C., Wilde, S.A., Guo, J.H., Cawood, P.A., Sun, M., Li, X.P., 2010. Single zircon grains record two Paleoproterozoic collisional events in the North China Craton. Precambrian Res. 177, 266–276.
Zhong, C.T., Deng, J.F., Wan, W.S., Mao, D.B., Li, H.M., 2007. Magma recording of Paleoproterozoic orogeny in central segment of northern margin of North China craton: geochemical characteristics and zircon SHRIMP dating of S-type granitoids. Geochimica 36 (6), 633–637.
Zhong, C.T., Deng, J.F., Wu, Y.P., Mao, D.P., Xi, Z., Chen, B., 2006. Geochemical characteristics and tectonic significations of Paleoproterozoic strongly peraluminous granitoids in the central segment of the northern margin of the North China craton. Geol. Bull. China 25 (3), 389–397.
Zhou, X.W., Zhao, G.C., Geng, Y.S., 2010. Helanshan high-pressure pelitic granulites: petrological evidence for collision event in the Western Block of the North China Craton. Acta Petrological Sinica 26, 2113–2121.

Please cite this article in press as: Guo, J., et al., UHT sapphirine granulite metamorphism at 1.93–1.92 Ga caused by gabbronorite intrusions: Implications for tectonic evolution of the northern margin of the North China Craton. Precambrian Res. (2011), doi:10.1016/j.precamres.2011.07.020